Journal of Geophysical Research: Solid Earth

RESEARCH ARTICLE
10.1029/2017JB014616

Key Points:
- We discuss a possible association between early twentieth-century earthquakes and oil production in California
- Coulomb stress modeling reveals significant stress changes at depths of ~5 km associated with oil production
- Rupture lengths of production-induced earthquakes might be limited by the small scale of stress-change lobes

Supporting Information:
- Supporting Information S1

Correspondence to:
S. E. Hough,
hough@usgs.gov

Citation:
Hough, S. E., & Bilham, R. (2018). Revisiting earthquakes in the Los Angeles, California, basin during the early instrumental period: Evidence for an association with oil production. *Journal of Geophysical Research: Solid Earth*, *123*, 10,684–10,705. https://doi.org/10.1029/2017JB014616

Received 26 JUN 2017
Accepted 1 OCT 2018
Accepted article online 19 NOV 2018
Published online 6 DEC 2018

Revisiting Earthquakes in the Los Angeles, California, Basin During the Early Instrumental Period: Evidence for an Association With Oil Production

Susan E. Hough[1] **and Roger Bilham**[2]

[1]United States Geological Survey, Pasadena, CA, USA, [2]CIRES, University of Colorado, Boulder, CO, USA

Abstract A total of seven independent $M_L \geq 4.0$ earthquakes occurred in the Los Angeles, California, basin, during the early instrumental period between 1932 and 1952, the largest of which was the 1933 Long Beach earthquake. Revising available macroseismic and instrumental data for a total of 6 $4.0 \leq M_L \leq 5.1$ events between 1938 and 1944, we conclude that early instrumental locations can be grossly inconsistent with detailed macroseismic data. We use available macroseismic data to revisit event locations. We further present evidence that most if not all of these moderate earthquakes may have been induced by oil production. We quantify the predicted stress change associated with production from eight oil fields in the southwestern Los Angeles basin and show that frictional failure would have been encouraged beneath and at the periphery of high-volume fields, with stress changes upward of 0.1 MPa at 5-km depth. The results suggest that if earthquakes are induced by stress changes associated with production, the magnitudes of events might tend to be limited by the limited spatial extent of lobes of increased Coulomb failure stress. It further appears that the advent of fluid injection recovery methods (*water-flooding*) around 1960 mitigated induced earthquake risk considerably.

Plain Language Summary We reconsider the locations and magnitudes of six moderate earthquakes that occurred in the Los Angeles region between 1935 and 1950. We show that, while these earthquakes were recorded by early seismometers, detailed damage observations provide a better indication of locations than do limited instrumental data. We further present evidence for an association between these earthquakes and oil production during the oil boom that began in the late 1930s. Using available industry data and established computation methods, we show that by the 1930s, oil production would have perturbed significantly the stress and faults in proximity to major fields at depths of 3–5 km. We suggest that the extent and therefore magnitude of induced earthquakes would have been generally limited by the spatially complex patterns of stress change. We further suggest that induced earthquake risk was mitigated significantly by the advent of so-called secondary recovery methods, whereby water was reinjected into fields to compensate for oil extraction.

1. Introduction

Hough and Page (2016) presented evidence that a number of the damaging moderate earthquakes in the Los Angeles basin in the early twentieth century might have been induced by oil and natural gas production. They considered earthquakes during the preinstrumental era in southern California (prior to 1932) as well as the 11 March 1933 M_w6.4 Long Beach earthquake. Moving forward into the early instrumental era, a total of six independent $M_L \geq 4.0$ earthquakes occurred over the 11 years following the Long Beach earthquake (Table 1 and Figure 1). While Hauksson et al. (2015) concluded that there was no evidence for significant induced earthquakes in the Los Angeles basin through the twentieth century, their study relied on instrumental locations and considered only overall seismicity distributions. In this study we focus on a detailed investigation of the larger events during the early instrumental era in the Los Angeles basin.

Apart from the Long Beach earthquake, the most notable earthquakes during the early instrumental period was a pair of moderate earthquakes that occurred in the southwestern Los Angeles basin, at 06:57 (UTC) on 22 October and 08:41 (UTC) on 14 November. Both earthquakes occurred close to midnight local time but were widely felt across the Los Angeles region. The second of these two earthquakes was stronger, causing damage estimated at $350,000–$1,000,000 ($6–$16 M in 2017 dollars) in the towns of Torrance and Gardena, and surrounding oil fields (Coast and Geodetic Survey [CGS], 1941; Los Angeles Times, 1941a,

Table 1
M4+ Earthquakes, Not Including Aftershocks, in the Los Angeles Basin Between 1935 and 1944

Year	M	D	Location	M_L	Reference
1935	12	25	Huntington Beach33.664°N, 117.964°W	4.3	No damage; small objects displaced in Huntington Beach (CGS, 1937; Los Angeles Times, 1935; Table S1).
1938	08	31	Keystone33.829°N, 118.277°W	4.4	Heavy cabinet fell and plaster cracked in Keystone; (CGS38; Neumann, 1940; LAT, 1938; Table S2).
1939	12	27	Terminal Island33.755°N, −118.260°W	4.5	Tiles fell in Terminal Island; plaster cracked in Long Beach and Huntington Park (Los Angeles Times, 1939, CGS39; Table S3).
1940	10	11	Keystone33.829°N 118.277°W	4.7	Plaster and chimneys cracked in Keystone; some plaster cracked in Gardena, Long Beach, and Redondo Beach (CGS40; Neumann, 1942; Table S4).
1940	11	01	Keystone33.829°N 118.277°W	4.1	Presumed aftershock of 11 October earthquake. Most strongly felt in Keystone. (Table S5).
1941	10	22	Dominguez Hills33.873°N 118.261°W	4.7	Table S6
1941	11	14	Torrance33.835°N 118.316°W	5.1	Tables S7 and S8
1944	06	19	Rosecrans33.90°N 118.274°W	4.4	Table S9

Note. Year, month (M), day (D), location, and magnitude of independent magnitude 4 and larger earthquakes in the Los Angeles basin between 1935 and 1944. The list includes six potentially independent events as well as two likely dependent events (1 November 1940 and 14 November 1941).

1941b; Ulrich, 1942; Neumann, 1946; Figure 1). The rate of independent $M_L \geq 4.0$ earthquakes in the region shown in Figure 1, roughly one event every 2 years between 1935 and 1944, was higher than the rate between 1945 and 2016 (roughly 1 event per 7 years). We note that while Hauksson et al. (2015) concluded that there was no evidence for widespread induced earthquakes in the Los Angeles basin in the twentieth century, Figure 1 of that paper also indicates a higher rate of $M \geq 2.5$ seismicity between 1935 and 1945 compared to later decades, which, as discussed later, cannot be explained as aftershocks of the 1933 Long Beach earthquake.

In this study we first visit the independent earthquakes between 1935 and 1944 (Figure 1), as well as the 14 November 1941 earthquake, which was likely a dependent event (i.e., triggered by the 22 October event). All

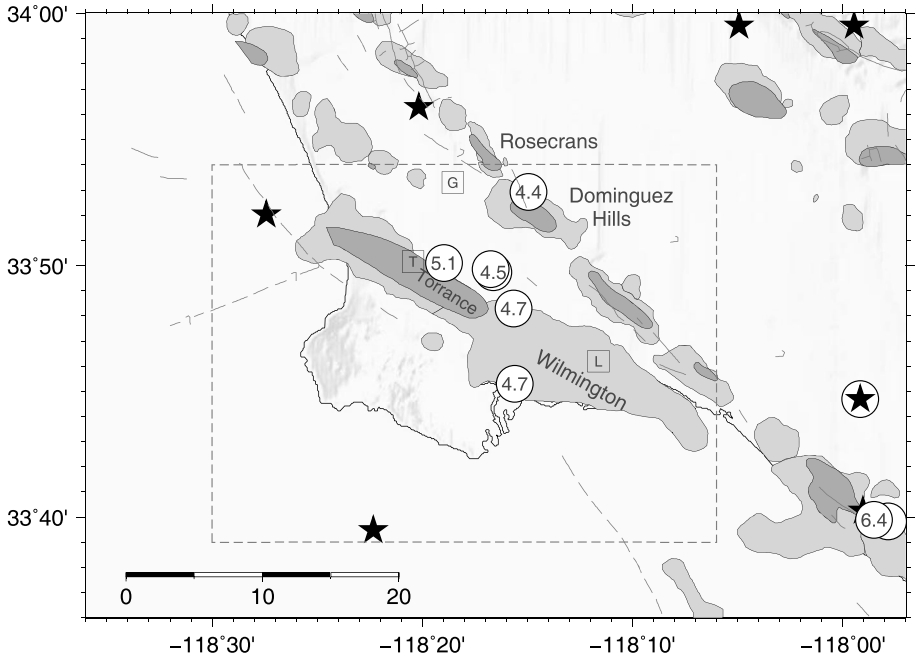

Figure 1. Map showing modern catalog locations of six independent $M_L > 4$ earthquakes between 1935 and 1944 (circles with event magnitudes indicated) and six later earthquakes between 1945 and 31 December 2016 (black stars). Mapped extent of zones of oil production in 1930 (darker gray shading; Barnes & Bowes, 1931) and in the present time (light gray shading; see Hauksson et al., 2015) is also shown. The squares indicate city locations: Gardenia (G), Torrance (T), and Long Beach (L). The dashed region corresponds to area shown in Figure 7. Parameters for earthquakes shown are given in Table 1. Regional faults in this and other figures from Jennings (1994).

but one of these earthquakes occurred within the inset region in Figure 1. We first use available macroseismic and instrumental data to revisit the locations and magnitudes of the earthquakes listed in Table 1. Although detailed analysis of intensity data became less common following the advent of instrumental monitoring, spatially rich felt and damage reports are available for these early instrumental earthquakes. We focus initially on the October and November 1941 earthquakes to illustrate our methodology.

We further explore a possible association between the earthquakes analyzed in this study and oil production in the southwest Los Angeles basin. The association of both seismicity and surface subsidence with oil extraction is not new and has been described in numerous regions (e.g., Frohlich & Davis, 2002; Kovach, 1974; Segall, 1989, 1992; Simpson & Leith, 1985; Suckale, 2010; Zoback & Zinke, 2002). Within the Los Angeles basin, a number of small but damaging shallow earthquakes occurred in the Wilmington oil field, starting in 1947, with subsequent events in 1949, 1951, and 1955; these events, which were recognized to have been associated with subsidence, were described by Richter (1958) and analyzed in detail by Kovach (1974; also see Frame, 1952).

In the early years of oil production (1928–1950), subsidence in the Los Angeles harbor region associated with the Wilmington oil field became increasingly problematic (e.g., Los Angeles Times, 1950). By 1948 the U.S. Navy publically voiced concerns about the impact on their operations in the adjacent harbor regions (e.g., Los Angeles Times, 1948). Initial proposals from the Navy to address the problem were not successful (e.g., Los Angeles Times, 1949). By 1955, Long Beach City officials joined the Navy in calling for programs to halt the still-increasing subsidence (Los Angeles Times, 1955); in late 1957, proposed State legislation aimed at halting subsidence drew opposition from major oil producers (Los Angeles Times, 1957). By 1958, however, agreement was reached to begin a *crash* repressurization program in the Wilmington field, with the dual objectives of increasing oil production and reducing subsidence (Los Angeles Times, 1958). This program involved the adoption of wide-spread water-flooding methods, whereby water was injected into fields to balance subsurface pressures; this method not only helped maintain subsurface pressures but also provided an important secondary recovery technique that improved production from fields as they become progressively depleted.

The deformation processes that accompanied initial oil-field operations prior to the late 1950s (e.g., Gilluly & Grant, 1947), combined with available reports of oil and coproduced water volumes, provide a rich source of data for examining possible earthquake triggering processes. We compare the inferred locations of the earthquakes determined in this study with the approximately predictable strain-fields quantified from fluid extraction, location, and depth information. We describe the dilatational strains above and below simple producing horizons and demonstrate how contiguous fields interact. We then examine the Coulomb failure conditions anticipated from the mapped oil fields and their extracted fluid volumes prior to known earthquakes. For each earthquake we compare the nearby strain-fields inferred from oil-extraction. Finally, we summarize the spatial and temporal association of known earthquakes with our predicted regions of enhanced Coulomb failure.

2. Materials and Methods

2.1. Data Sources for Earthquakes During the Early Instrumental Era

The cluster of earthquakes between 1935 and 1944 (Figure 1) occurred during the early instrumental era in Southern California, a period for which some instrumental data were collected by a sparse network of Wood-Anderson instruments, but for which clock errors were potentially substantial and largely irreducible, and the network was especially sparse (see Hutton et al., 2010). Additional stations were installed in 1952, and timing improved considerably with the introduction of WWVB signals in 1963. Epicentral locations determined from early instrumental data are not expected to be accurate (see Hutton et al., 2010), even using modern relocation methods, due to fundamental data limitations. Hutton et al. (2010) estimated nominal HYPOINVERSE (Klein, 2002) uncertainties for most of the $M \geq 3$ events within the network from 1932 to 1973 to be less than 6 km; this conclusion has never been tested using detailed damage data.

During the early instrumental period macroseismic data were collected routinely by the Coast and Geodetic Survey (CGS) as part of its seismological program in the western United States (e.g., Ulrich, 1938). Macroseismic information describing effects of shaking on structures and people was collected under what was known as the Questionnaire Program, whereby postcard questionnaires—essentially the same as the

questionnaires used later by the U.S. Geological Survey "Did You Feel It?" (DYFI) system (Wald et al., 1999)—were sent to postmasters following notable felt earthquakes (Ulrich, 1938). The program was strengthened during 1937 with the transfer of an employee from the Washington D.C. office to San Francisco (Ulrich, 1938). Extensive preliminary summaries were published by the CGS in the publication series, "Abstracts of Earthquake Reports" (e.g., Coast and Geodetic Survey [CGS], 1941). This information can be supplemented by newspaper articles published in the aftermath of the earthquakes as well as other sources (Tables S1–S9).

Strong motion monitoring in the Los Angeles region began in 1932 (Ulrich, 1935). Twelve triggered accelerographs were installed by the CGS in the greater metropolitan region by 1935; print copies of records and estimated PGA values were published in annual CGS reports. Hudson et al. (1975) presents Fourier spectra computed from digitized records of the 14 November 1941 earthquake (see Data and Resources).

2.2. Modeling

We use standard modeling methods to explore the hypothesis that earthquakes analyzed in this study were induced by oil production in the Los Angeles basin. Analytic formulations for displacement and stress changes surrounding compacting poroelastic production fields were derived by Segall (1989). The triggering potential of poroelastic stress change on nearby faults has been explored by a number of studies, including Soltanzadeh and Hawkes (2009), who consider predicted stress changes from both injection and production and showed that in a compressional regime, faults above and below a production horizon tend toward reactivation. We use established boundary element methods constrained by available industry data to examine Coulomb failure conditions (e.g., King et al., 1994; Toda et al., 1998) in the region surrounding the Willmington field and other oil fields in the southwestern Los Angeles basin.

3. Results

3.1. The 22 October and 14 November 1941 Earthquakes

3.1.1. Intensities and Locations

Neumann (1946) provides intensity assignments, including *not felt* reports (MMI 1) at a total of 108 and 163 locations, respectively, for the October and November earthquakes; intensity values are available from the Earthquake Intensity Database maintained by the National Oceanic and Atmospheric Administration (NOAA). Additional information are provided by Coast and Geodetic Survey (CGS; 1941), including summaries of effects at all locations and reports for a total of 140 and 182 locations, respectively. The additional accounts improve spatial sampling significantly (and provide an indication of population density at the time), providing accounts from specific street addresses throughout the cities of Long Beach and Los Angeles. Revisiting summarized accounts, we estimate modified Mercalli intensities that are typically, although not uniformly, one unit lower than the assignments by Neumann (1946; Tables S6 and S7). For example, while the NOAA database lists a maximum MMI 8 for the 14 November earthquake, we conclude that descriptions and photographs of damage are more consistent with a maximum MMI of 7 to at most 7.5 based on the report that "many of the damaged buildings showed that failure was due either to poor workmanship, poor design, or both" (Neumann, 1946; p. 17). Neumann (1946) assigns a maximum intensity of "7–8," which was apparently rounded up in the NOAA database. At other locations, MMI 6 was sometimes assigned for locations where small objects fell or were displaced, with no other documented damage such as cracking of plaster. At the low end of the scale, for all earthquakes the NOAA intensity database, presumably drawing from the U.S. Earthquake Report publications, lists a minimum MMI value of 3 for all locations where shaking was reported as felt. For these locations we assign values of 2 based on DYFI? data from recent earthquakes (Wald et al., 1999), which indicates that MMI 2 shaking is often weakly felt in populated areas even for earthquakes that occur at night.

The suggestion that intensities were systematically overestimated for U.S. earthquakes through the first half of the twentieth century is not new; Stover and Coffman (1993) reached the same conclusion. To some extent, this overestimation resulted from the practice of assigning a single value for a city based on the most severe documented effects, even when individual accounts from the same city clearly indicated lower values. The 22 October 1941 earthquake provides an illustrative example: Neumann (1946) gives MMI 6 for the cities of Los Angeles and Long Beach, while detailed accounts from both cities (Coast and Geodetic Survey [CGS], 1941) describe effects commensurate with intensities as low as 3–4. As discussed by Stover and Coffman (1993), early intensity assignments were also generally more based on subjective human reactions than on

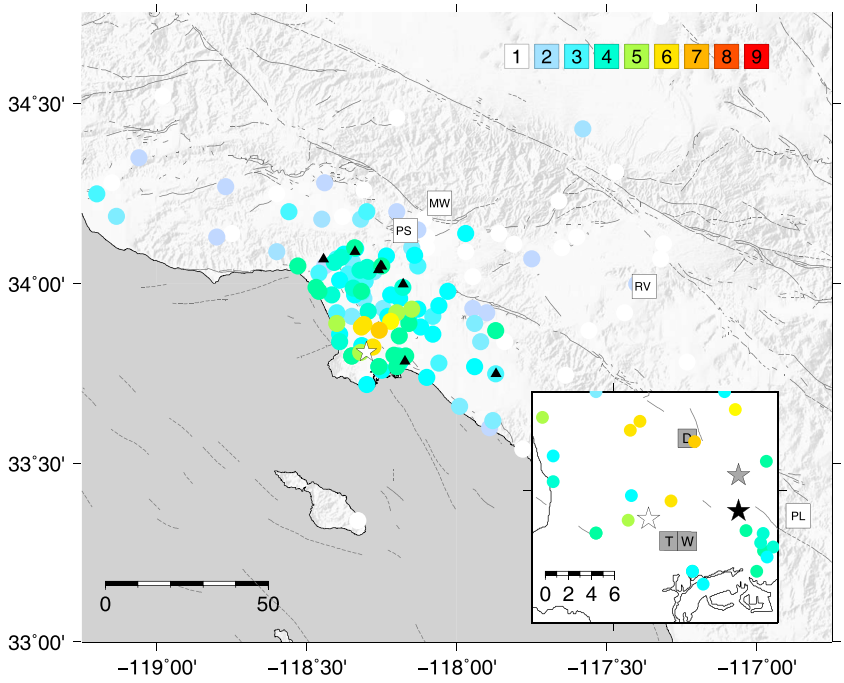

Figure 2. Reinterpreted intensity distribution (MMI color scale indicated) for the 22 October 1941 earthquake. (Original values listed in Table S6) Locations of Wood-Anderson stations are indicated with squares: PAS (PS), MWC (MW), RVR (RV), and PLM (PL); the black triangles indicate locations of strong motion stations that recorded the earthquake. The white star indicates modern catalog location. The gray squares in inset indicate sections (see Data and Resources) where active development of the Torrance (T), Wilmington (W), and Dominguez Hills (D) oil fields was concentrated in 1941 (note that these symbols indicate oil fields not city locations). In inset panel, the white, black, and gray stars indicate, respectively, the modern catalog location and the epicenters given byGutenberg (1943)andBravinder (1947).

documented effects on objects and structures, which in their view provided more reliable indicators of intensities higher than 4–5. The reinterpreted intensity values assigned in this study smoothly dovetail with available not felt reports (e.g., Figure 2), yielding a distance decay that is more consistent with intensity data from the DYFI system (Wald et al., 1999).

To better characterize near-field shaking from both earthquakes, we consider in detail additional sources of macroseismic information documenting damage, as well as details provided by Coast and Geodetic Survey (CGS; 1941) and Neumann (1946). For the 22 October earthquake, detailed damage information is limited. For this event, however, Bravinder (1947) presents a detailed description of offset oil wells along two south dipping, approximately east-west trending reverse faults, labeled W-1 and W-2 (Figure 3b), that are nearly parallel to the axial trend of the anticlinal fold within which the Dominguez oil field resides (Figure 3). Well tubing was reportedly offset by the earthquake at depths of ≈1.8 km (6,000′) in wells crossing faults W-1 and W-2. The zone of offset wells extended approximately 1 km east-west. The uppermost zone of well damage is at a depth of ≈0.5 km; the bottom of the zone is not constrained but extends to at least 1.2 km (Bravinder, 1947). Tubing in one well crossing fault W-1 was completely sheared at a reported depth of 5,320 feet, Bravinder (1947) concludes that the lateral component of movement of the W-1 fault was more than 18 cm (7 inch) at this location. Given the fault geometry, this implies fault slip of approximately 25 cm (10″) toward the upper edge of the rupture. The faulting mechanism in the 1941 earthquake is not constrained, but is presumed to be reverse. A rupture area of ≈1 km^2 and an average slip of 30 cm correspond to M_w4.6 assuming a shear modulus of 3×10^{10} N-m.

Bravinder (1947) suggests, presumably echoing the conclusion of Gutenberg, that the October earthquake nucleated on the Newport-Inglewood fault several kilometers southeast of the zone of damaged wells and that stress within the Dominguez Hills anticline was released as a secondary effect of the earthquake. Richter (1958; page 156) also notes that waveforms of this earthquake were of *normal character* in contrast to waveforms from shallow slumping events in the Wilmington area between 1947 and 1955 (see Kovach,

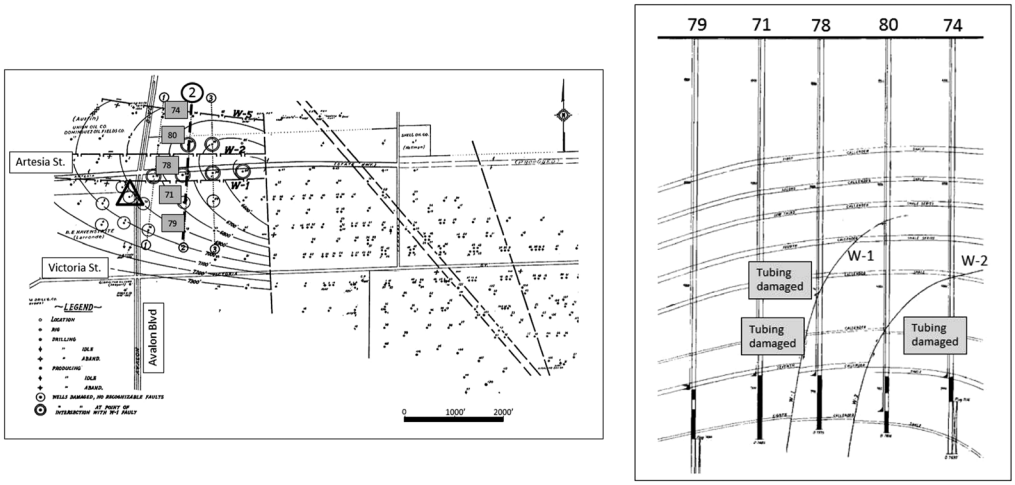

Figure 3. (a, left) The double circles indicate wells (labeled by number) within Dominguez Hills oil field that were damaged by the 22 October 1941 earthquakes and that intersect faults at depth; the single circles indicate damaged wells that were damaged by the earthquake but do not intersect recognizable faults. The triangle indicates location of initial well drilled in this part of the field in 1940. Well labeled 79 penetrated Franciscan Schist basement at a depth of 3.8 km in 1941. The dashed black line labeled 2 indicates cross section shown in Figure 3b. The dashed line in inset indicates extent of map region as well as the extent of the Dominguez Hills oil field as of 1930 (dark gray shading) and in modern times (lighter gray shading), and primary zone of well damage from the 22 October earthquake (horizontal black line, 1942). (b, right) Cross section, with well numbers labeled, indicating well damage at point of intersection with fault strands at depth (figures redrafted fromBravinder,1947).

1974). He further suggests that the earthquake occurred at the usual depth of about 16 km, although in retrospect depths were very poorly constrained during the early instrumental era. Given the extent of the zone of damaged wells and that the reinterpreted intensities are centered on this location, we conclude that the earthquake was centered very close to the zone of disturbed wells (33.873°N, 118.261°W), with a (relatively) shallow focal depth. This location is 6–7 km from the early and modern instrumental locations (Figure 4a). We note that while the estimate location of this earthquake is certainly not precise to 0.001° (or even 0.01°), in some cases, detailed damage information, including damage to oil wells (e.g., Figure 3) or a tight concentration of maximum damage, provides a basis for identifying a precise preferred epicenter. Formal epicentral location uncertainties are difficult to determine but are likely on the order of ±3–5 km.

The modern catalog location for the 14 November 1941 earthquake is within ≈2 km of the location estimated by Gutenberg (1943; Figure 5). For this earthquake, detailed accounts of damage are provided by contemporary news articles (Table S8) as well as Coast and Geodetic Survey (CGS), 1941 and Neumann (1946). We assign a total of 23 MMI values using news accounts for which a location can be identified from information provided. In most cases the location can be estimated to within 100 m, typically from a street address or specified street intersection. Other accounts describe rupture of two large tanks, one north of Torrance and a 55,000 gallon General Petroleum Corporation tank north of Wilmington (Los Angeles Times, 1941a). The additional information improves significantly the characterization of near-field intensities (inset, Figure 5) relative to the Neumann (1946) assignments.

Although the 14 November earthquake reportedly caused damage to oil fields near Torrance (Ulrich, 1942), according to Hamilton et al. (1969), documented damage was restricted to surface oil field installations. In addition to the reported collapse of two large tanks (Los Angeles Times, 1941a; Figure 5), two other large tanks buckled but did not rupture; while the location of these tanks is not specified, an article in the Los Angeles Times (1941a) notes that a single large tank was damaged in Wilmington, suggesting that the buckled tanks were in the tank farm north of Torrance.

The method presented by Bakun and Wentworth (1997) has been widely used to estimate locations and magnitudes from intensity data but cannot pinpoint epicenter precisely. For the 14 November earthquake we instead consider the detailed near-field intensity distribution (Figures 4b and 5). The heaviest

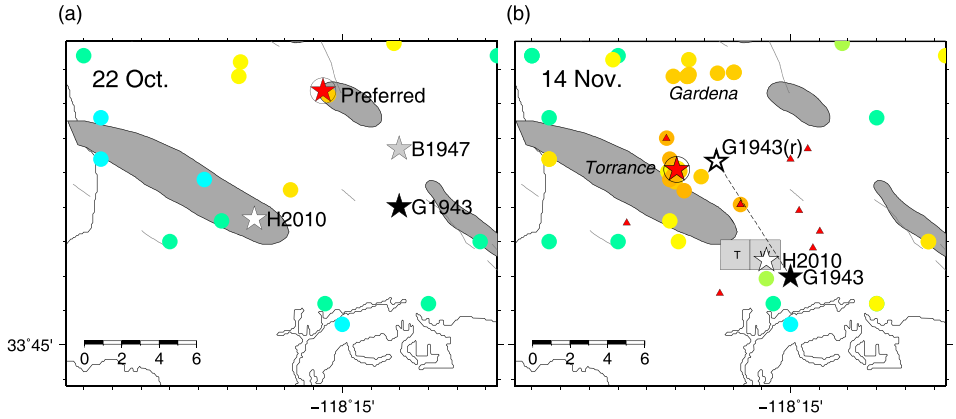

Figure 4. (a, left) Near-field intensities for 22 October 1941 earthquake (circles) with epicenters determined by Gutenberg (1943) (black star; G1943), Bravinder (1947) (light gray star; B1947), Hutton et al. (2010) (white star; H2010), and preferred epicenter (circled red star). The dark shaded regions indicate oil fields as of 1930 (Barnes & Bowes,1931). (b, right) Near-field intensities for 14 November 1941 earthquake (circles) with epicenters determined by Gutenberg (1943) (black star; G1943), Hutton et al. (2010) (white star; H2010), and this study (circled red star). The star labeled G1943(r) indicates G1943 epicenter relocated using mislocation vector (dashed black line) estimated from analysis of 22 October earthquake. The gray squares labeled T and W indicate Sections of Torrance and Wilmington oil fields under active development in 1941 (see Data and Resources). The small red triangles indicate oil tank farms, including two (underlain by colored circles) that were damaged by the earthquake.

concentration of damage was within the town of Torrance, >6 km northwest of the instrumentally constrained epicenters (Gutenberg, 1943; Hutton et al., 2010). The early and modern instrumental locations are considered implausible in light of (1) modest macroseismic effects in nearby communities, including Wilmington, and (2) the lack of damage to surface oil field installations in the Wilmington area, including

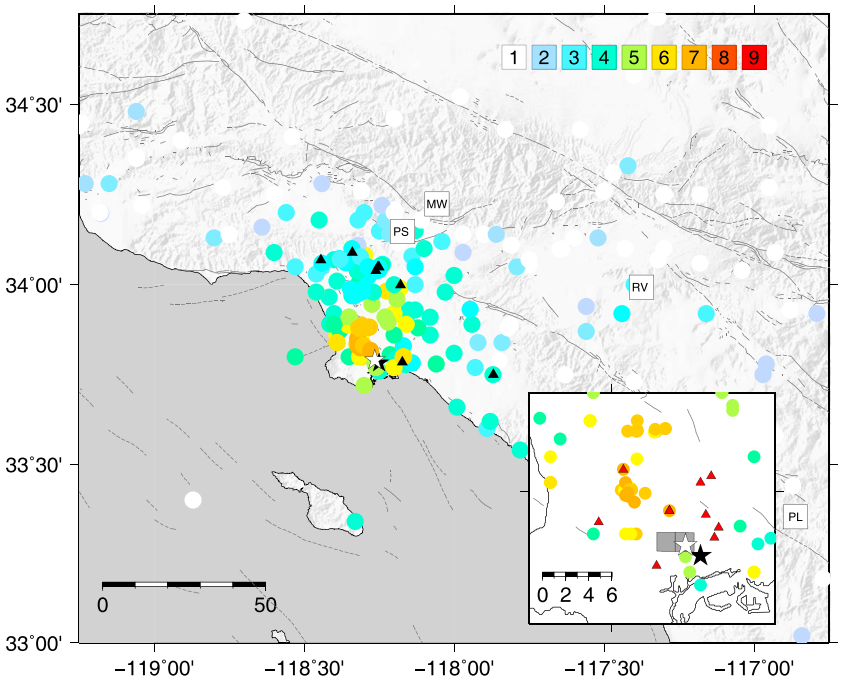

Figure 5. Intensity distribution (color scale indicated) for the 14 November 1941 earthquake. Locations of Wood-Anderson stations are indicated with squares: PAS (PS), MWC (MW), RVR (RV), and PLM (PL); the black triangles indicate locations of strong motion stations that recorded the earthquake. The white and black stars indicate modern catalog location and epicenter determined by Gutenberg (1943), respectively. The gray squares in inset indicate sections where active development of the Torrance and Wilmington oil fields was concentrated in 1941. The red triangles indicate locations of oil tank farms; in two of which (underlain by circles indicating MMI values) oil tanks collapsed.

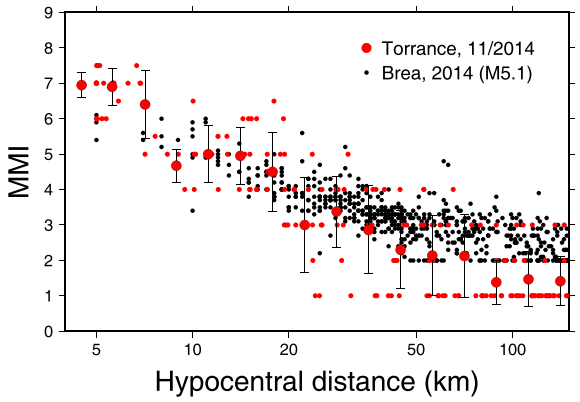

Figure 6. Raw and bin-averaged MMI intensities for the November 2014 Torrance earthquake (respectively, small red dots and large red dots including ±1σ) and raw Did You Feel It? intensities for a 29 March 2014 M_w5.1 earthquake in the Los Angeles area (black dots).

several oil tank farms (Figure 4b), apart from the one damaged oil tank ≈3 km northwest of the instrumental locations.

We conclude that the instrumental location based on limited early data is inconsistent with detailed damage data and that tight concentration of damage in Torrance provides the best indication of the epicenter of the 14 November event: 33.835°N, 118.316°W (Figure 4b). Again, we do not suggest that the epicenter can be determined to 0.001°; for this event, the preferred location is constrained to within ±2–3 km. Contemporary accounts consistently indicate that this was the hardest hit region, and within central Torrance, the tightest cluster of damage did not simply coincide with the locations of larger commercial and other structures (e.g., McDonald & Nessler, 1941). Also, although a handful of relatively high intensities are also estimated several kilometers north of this location in the town of Gardena (Figure 4b), contemporary sources consistently indicate that the overall damage was lower there than in Torrance. Following immediate surveys of damaged buildings, for example, it was estimated that building damage would not exceed $350,000 and $50,000 in Torrance and Gardena, respectively (Los Angeles Times, 1941b), and Neumann (1946) reported that chimney damage was less extensive in Gardena than in Torrance. The relatively severe damage in Gardena does, however, provide further evidence that the early and recent instrumental locations are not correct. That is, it is more likely that the epicenter was north of the city of Torrance, in the relatively sparsely populated area between Torrance and Gardena, than south of Torrance.

In addition to the macroseismic observations, one can reconsider the instrumental location determined by Gutenberg (1943) in light of the conclusions regarding the 22 October earthquake. The discrepancy between the location estimated by Gutenberg (1943) and the preferred location estimated by this study suggests that formal HYPOINVERSE uncertainties underestimate the true uncertainties of early instrumental event locations; the fact that modern instrumental locations are no better suggests that clock errors prior to the advent of WWVB timing (see Hutton et al., 2010) rather than analysis techniques are the largest source of uncertainty for earthquakes during the early instrumental period. Interestingly, applying the mislocation vector inferred for the 22 October earthquake (i.e., between the Gutenberg, 1943, location and the preferred location from this study) to the 14 November earthquake yields an epicenter of 33.839°N, 118.293°W, within 2 km of the epicenter estimated from macroseismic observations (Figure 4b). Although apparently systematic (inferred) errors could be coincidental, we conclude that at a minimum, locations estimated from early instrumental data are grossly inconsistent with detailed damage data, and, arguably, both instrumental and detailed macroseismic observations support the preferred epicenter shown in Figure 4b.

3.1.2. Magnitudes

One can also use available strong motion and macroseismic data to calculate improved magnitude estimates for early instrumental earthquakes. Applying the BW97 method using the attenuation relationship of Bakun (2006) and assuming the preferred epicenters for both earthquakes yield 4.0 and 4.5, respectively, for the 22 October and 14 November 1941 earthquakes. These values are lower than the instrumentally constrained M_L estimates, 4.7 and 5.1. This could indicate that the intensities were not commensurate with magnitude because the events had low stress drop (Hough, 2014). The discrepancy could also, however, be a consequence of using reinterpreted intensities for this event together with the calibration relationship from Bakun (2006), which is derived using intensity data from a mixture of older and recent calibration events without attempt to uniformly reconsider original intensity assignments. A third possibility is that the instrumentally determined magnitudes are too high.

The magnitude estimates can also be reconsidered by comparing both macroseismic and instrumental data with data from recent earthquakes. We compare intensities for the November earthquake determined by this study with DYFI intensities for a M_w5.1 earthquake that occurred at estimated 5.1-km depth near the town of Brea in the Los Angeles region on 29 March 2014 (Figure 6). To calculate hypocentral distances for the 14 November 1941 earthquake, we assume a nominal depth of 5 km. The range and mean intensities for the two events are similar, as is the overall felt extent. The reinterpreted intensity values do suggest a

Table 2
Strong Motion Recordings of 22 October and 14 November 1941 Earthquakes

Location	Lat.	Long.	D_1	PGA_1	D_2	PGA_2
Long Beach	33.76	118.24	13	0.32	15	0.49
Vernon	33.995	118.200	16	0.17	20	0.19
Los Angeles Edison Bldg	34.050	118.254	21	0.09	21	0.09
Los Angeles Chamber of Commerce	34.0388	118.2607	20	0.18	20	0.14
Los Angeles Subw. Terminal Bldg	34.049	118.250	21	0.09	21	0.07
Westwood	34.069	118.444	29	0.05	26	0.09
Hollywood Storage Bldg	34.0896	118.3390	27	0.06	25	0.06
Hollywood Storage, nearby lot	34.0896	118.3390	27	0.06	25	0.08
Santa Ana Courthouse	33.750	117.869	–	–	46	0.06

Note. D_1 and D_2 indicates epicentral distances in kilometer assuming preferred locations for the 22 October 1941 and 14 November 1941 earthquakes, respectively; PGA_1 and PGA_2 indicate reported peak ground acceleration in m/s^2 for the 22 October 1941 and 14 November earthquakes, respectively (Neumann, 1946).

relatively shallow source and possibly low stress drop for the 14 November 1941 earthquake, with high near-field intensities and a relatively steep decay of intensity values with distance (Hough, 2014). Given the uncertainties, however, and the fact that the 1941 earthquake occurred shortly after midnight local time, this result is not considered robust. We conclude that, overall, the macroseismic intensities for the November 1941 earthquakes are consistent with the instrumentally determined magnitude (M_L5.1; Hutton et al., 2010).

Both the 22 October and 14 November earthquakes were additionally recorded by a number of CGS strong motion instruments Peak ground acceleration (PGA) values from basement and free-field instruments are given in Table 2 (Neumann, 1946) The highest recorded PGA for the 14 November, 0.49 m/s/s, was recorded in Long Beach. Recorded PGA values are consistent with, although somewhat lower than, PGA values from the 29 March 2014 *M*5.1 earthquake, which was well recorded instrumentally across the Los Angeles basin (Figure 7a). Neumann (1946) notes that three of the recordings with relatively low PGA values, all at distances of 20–26 km, might have been preceded by stronger motion. PGA values for the 22 October earthquake are slightly lower than PGA values from the other two events, with fewer stations triggered (Figure 7a). We conclude that while sparse, the available strong motion data as well as macroseismic data support the instrumentally determined magnitudes for both 1941 earthquakes.

Hudson et al. (1975) presented Fourier spectra calculated from digitized recordings of the 14 November 1941 earthquake at two stations, including Long Beach. The (triggered) accelerograms were digitized using the semiautomatic procedure described by Hudson et al. (1975). Integrating the acceleration record from the Long Beach station yields the velocity records shown in Figure 7b. The velocity records are dominated by large-amplitude arrivals that follow the (presumed) *S* wave arrivals by ≈5 s. The arrivals are qualitatively consistent with basin-generated surface waves (e.g., Frankel et al., 1991; Graves et al., 1998); however, the large amplitude and long-period nature of these arrivals, from an earthquake at a distance of only about 15 km, suggests a relatively shallow source (i.e., approximately 5–6 km). While limited, available strong motion as well as macroseismic data provide further evidence that the 14 November 1941 was an especially shallow event; strong motion data also support the catalog magnitude estimate of M_w5.1.

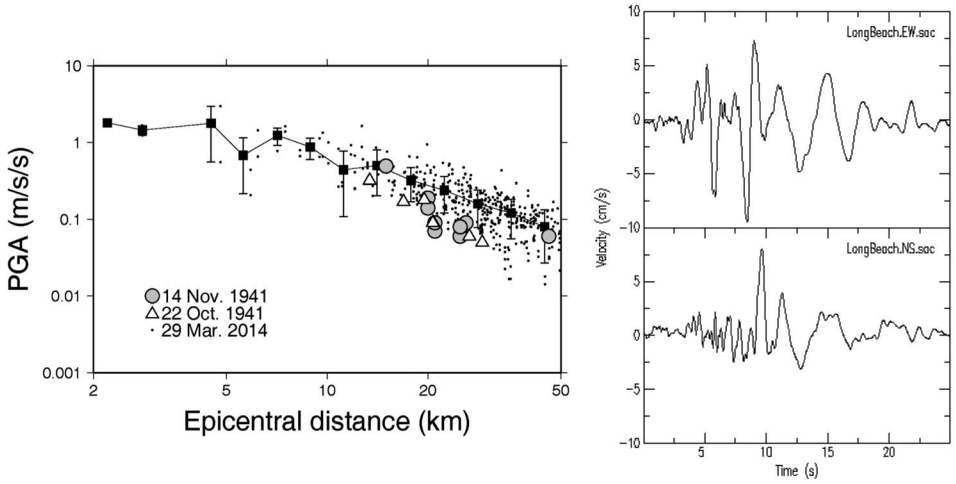

Figure 7. (a, left) Raw and bin-averaged peak ground accelerations (PGAs; including ±1 standard deviation) for the 29 March 2014 M_w5.1 earthquake (black dots and black squares, respectively) and reported PGA values for the 22 October and 14 November 1941 earthquake (white triangles and gray circles, respectively). (b, right) Horizontal components of motion (velocity) during the 14 November 1941 earthquake recorded in Long Beach (Hudson et al., 1975).

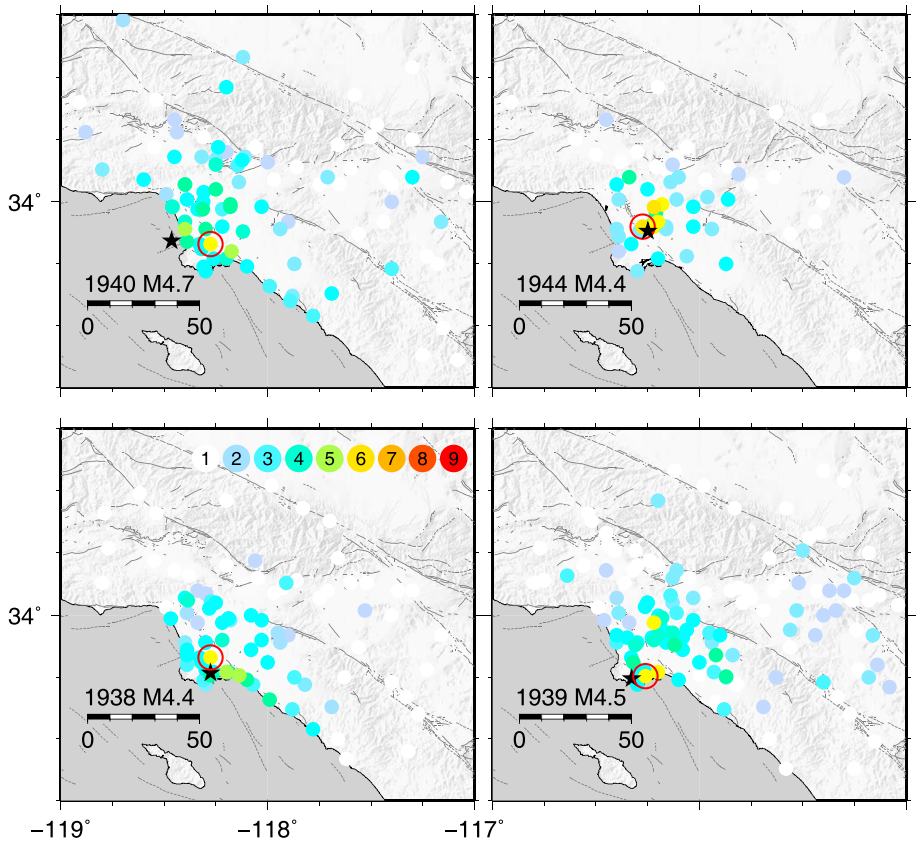

Figure 8. Intensity distribution (color scale indicated in lower left panel) for moderate earthquakes in 1938 (lower left), 1939 (lower right), 1940 (upper left), and 1944 (upper right). The black stars in each panel indicate modern catalog locations; the open red circles indicate preferred locations, corresponding to locations where the most severe effects were reported for each event (this study).

3.2. Additional Earthquakes

We further reconsider the intensity distributions for five of the other earthquakes in Table 1. Felt reports are especially limited for the 25 December 1935 earthquake; we do not attempt to relocate this event. For the other four independent earthquakes, reinterpreted intensity values are shown in Figure 8. None of the earthquakes listed in Table 1 caused more than very light damage; news articles provide little additional detail beyond the CGS reports (Coast and Geodetic Survey [CGS], 1940, 1941, 1942, 1944).

In light of the conclusions regarding the 1941 earthquakes, and the mismatch between modern instrumental epicenters and most severe effects evident in Figure 4, we consider detailed macroseismic observations to refine preferred locations for the other moderate earthquakes in Table 1. Brief summaries of effects are listed in Table 1; in Figure 4, the location with the strongest reported effects is circled. We conclude that again, the early instrumental locations are inconsistent with the detailed damage information (for some events more than others) and that the sites of most severe effects provide the most reliable epicentral locations for the 1938, 1939, and 1940 earthquakes (Table 1 and Figure 8).

Among the other events (Figure 8), the 19 June 1944 earthquake merits further discussion. This event caused light damage, including cracked plaster and cracked chimneys, with a PGA of over 10%*g* (1.10 m/s^2) recorded at one station (Bodle, 1946; Table 3 and Figure 9). An initial earthquake, at 17:03 LT on 18 June was followed by a second event at 20:06 LT the

Table 3
Recorded Peak Ground Accelerations (m/s^2), 19 June 1944 Earthquake

Location	Lat.	Long.	PGA
Long Beach	33.76	118.24	0.25
Vernon	33.995	118.200	1.10
Los Angeles Edison Bldg	34.050	118.254	0.12
Los Angeles Chamber of Commerce	34.0388	118.2607	0.19
Los Angeles Subw. Terminal Bldg	34.049	118.250	0.18
Hollywood Storage Bldg	34.0896	118.3390	0.10
Hollywood Storage, nearby lot	34.0896	118.3390	0.09

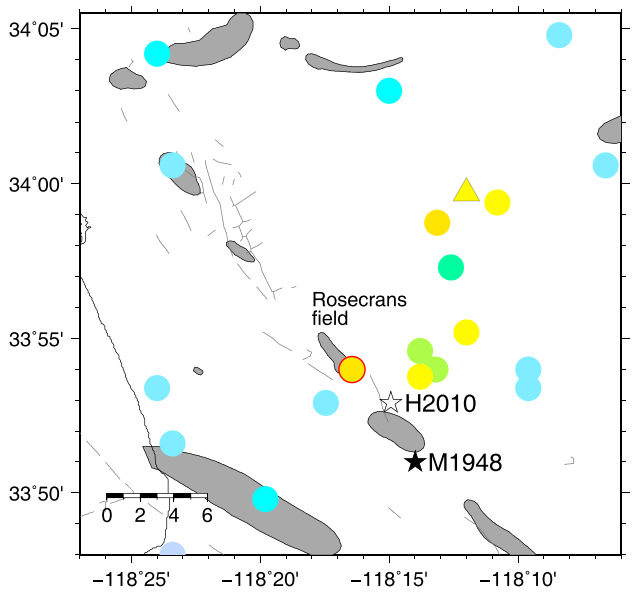

Figure 9. Near-field intensities for 19 June 1944 earthquake (circles; location of well damage circled in red) with epicenters determined by Martner (1948) (black star; M1948) and Hutton et al. (2010) (white star; H2010). The triangle indicates instrumental intensity from Coast and Geodetic Survey station Vernon. The shaded regions indicate oil fields as of 1930.

same day; although the catalog magnitudes are close (M_L4.4 and M_L 4.3), news accounts as well as strong motion data indicate that the first earthquake was significantly stronger. Macroseismic effects are described in detail for both events independently; there is no indication that effects were conflated (Bodle, 1946). Unlike the earthquakes in 1938, 1939, and 1940, notably severe effects were not concentrated in a single location (Figure 9). This earthquake also damaged wells in the Rosecrans oil field (Martner, 1948; Figure 10). In this case, wells were damaged by slip over an ≈800 m extent of an east striking, south dipping reverse fault. Martner (1948) concluded that the amount of movement in the wells was generally less than several inches. A rupture length and width of 800 m and average slip of 7–12 cm corresponds to M_w 3.5–3.6, smaller than the instrumentally estimated magnitude (M_L4.4).

It thus appears that the documented zone of well damage does not indicate the primary rupture of the 19 June 1944 event. Like both of the 1941 earthquakes, the early instrumental location (Martner, 1948) is implausibly far south, yet for this event the notably high PGA and the most severe damage are even farther (over 10 km) from the instrumental location. The overall intensity pattern poses a further enigma, with a distributed zone of high intensities but a smaller overall felt extent than the other earthquakes of comparable magnitude. One plausible explanation for the seemingly inconsistent data is that either an initial event within or very close to the location of well damage in the Rosecrans field was followed quickly by a larger mainshock ≈10 km northeast, or an initial event could have triggered a shallow earthquake in the Rosecrans field. Closely spaced events would be impossible to distinguish with a combination of early weak and strong motion data.

Preferred locations for all earthquakes analyzed in this study are shown in Figure 1; the location of the 1944 event is especially uncertain. Figure 11 presents macroseismic data for all events in Table 1, not including the 1935 earthquake, averaged in logarithmic distance bins. To calculate distance for the 1944 earthquake, we assume an epicenter of 33.95°N, 118.25°W. This comparison suggests that the 1938, 1939, 1940, and

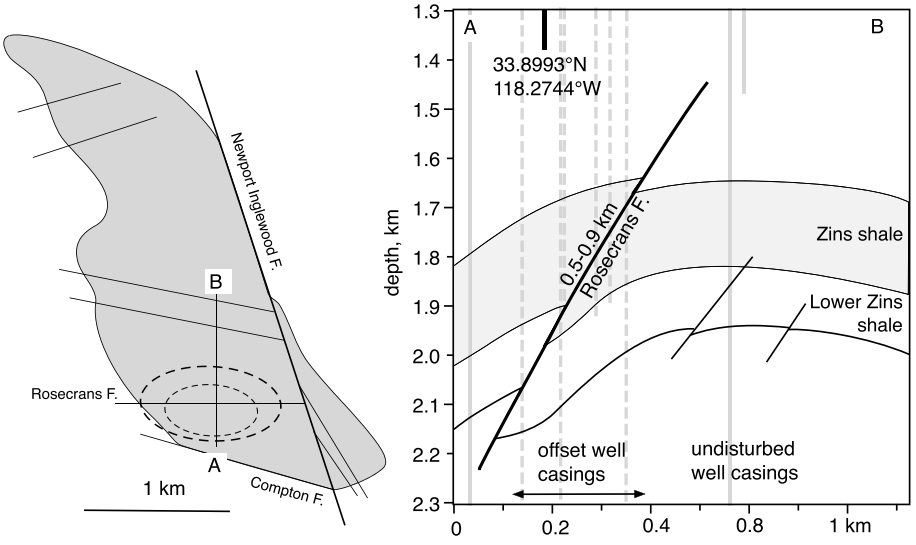

Figure 10. Maps indicating (left) spatial and (right) depth extents of documented well damage in the Rosecrans field following the 19 June 1944 earthquakes (recrafted from Martner, 1948). Larger oval on map (left) indicates overall extent of well offset; smaller oval indicates zone of well damaged at point of intersection with Rosecrans fault. The indicated subkilometer rupture length of the Rosecrans fault is estimated from unbroken wells to east and west.

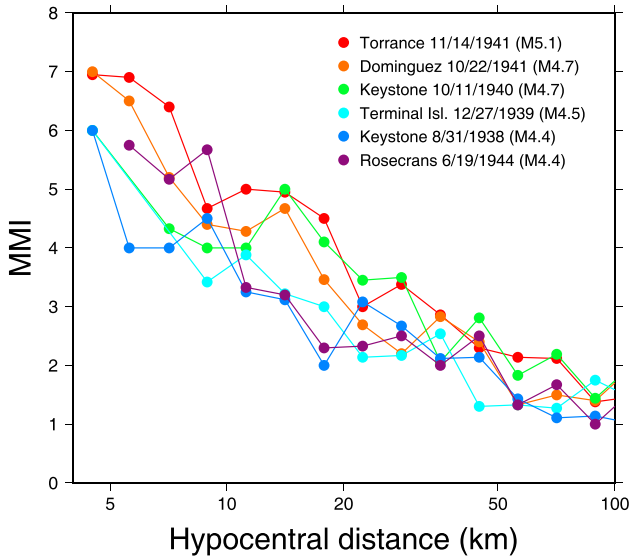

Figure 11. Bin-averaged intensity data for the events listed in Table 1, not including the 1935 earthquake, assuming preferred event locations from this study (see text for discussion of 1944 event location).

1944 earthquakes were of comparable magnitude, and all smaller than the 14 November earthquake. The reinterpreted intensity data are generally consistent with the instrumental magnitudes; we conclude that there is no basis for reconsidering the instrumental magnitude estimates for any of the events. As discussed earlier, the 1944 earthquake remains enigmatic: apart from the distributed MMI 5.5–6 zone, intensities are generally lower than those from the other events. A shallow source depth could account for high near-field intensities (e.g., Hough, 2014), but the strongest shaking would be expected to be tightly concentrated. Among the events analyzed, the 11 October 1940 earthquake might have been relatively deep: the near-field effects were relatively modest, but shaking was relatively strongly felt at larger distances.

3.3. Spatial/Temporal Association of Earthquakes and Oil Fields

The spatial association between our preferred event locations and active oil fields (Figure 1) motivated us to further consider both the spatial and the temporal association between the earthquakes analyzed in this study and industry activities. Within the inset region shown in Figure 1, six independent M_L4.4–5.1 earthquakes occurred between 1938 and 1944, while only two earthquakes occurred within the same region between 1945 and 2016. If the earthquakes between 1938 and 1944 were aftershocks of the 1933 Long Beach event, they should follow Omori's law (Omori, 1894). A timeline of events within this region, however, reveals a steady decay through the end of 1938 followed by an increase in rate beginning in 1939 (Figure 12). Moreover, no $M_L \geq 4.0$ earthquakes occurred in this region between 1945 and 1970 and, while, the preinstrumental catalog is less well constrained, none of the $M_L \geq 4.0$ earthquakes analyzed by Hough and Page (2016) are within this region. We conclude that the rate of moderate earthquakes in the southwestern Los Angeles basin was elevated (relative to the rest of the twentieth century) between 1938 and 1944 and cannot be explained as aftershocks of the 1933 Long Beach earthquake.

An alternative explanation for the cluster of earthquakes between 1938 and 1944 is that some if not most of them were induced by oil production. We first consider in detail the pair of moderate earthquakes in 1941.

3.3.1. The 22 October and 14 November 1941 Earthquakes

The evidence presented in this study, that is, that the 22 October 1941 earthquake occurred at shallow depth within or very close to the Dominguez Hills field, provides a direct indication that this earthquake might have been induced by oil production. Even if one rejects the conclusion that the epicenter was at relatively shallow depths and very close to the zone of observed well damage within the field, the strongest shaking was clearly centered around this location. The Dominguez Hills oil field was discovered in 1923; water-flooding, or secondary oil recovery involving injection of water into fields, began in 1947 (Barnds, 1964). Between 1935 and 1942, production in the field was fairly steady, ranging from 3.4 to 5.4 million barrels every 6 months (see Data and Resources). According to Huguenin (1939, pp 44–45), "Probably the most outstanding development" of the period ending June, 1940, was the completion of the most westerly outpost well nearly 0.37 km (1200′) west of the nearest producer, "on the west side of Avalon Blvd approximately 1650 feet north of Victoria Street," (see Figure 3a) striking oil at 2.1 km (6980′). This well is within a few hundred meters of the inferred rupture of the 22 October earthquake. During the first half of 1941, the zone shown in Figure 3a remained the principal area of development and production in the field. As of 1941, production zones were between 1.1 to 2.3 km (3,900–7,500′; Bravinder, 1947). One test well, Union Oil Company's Callender No. 79 (API 03707058; see Data and Resources), located at 33.869594°N, 118.262975°W (Figure 3), penetrated the Franciscan schist basement in February 1941 at a depth of 3.78 km (12,415′) and was plugged to a depth of 2.28 km (7490′) in September 1941 (Figure 3; Bravinder, 1947, also see Data and Resources). If the dip of the W-1 fault continues at depth, it is likely that the Callender No. 79 well intersected the fault at depth. Both the spatial association with the field and the temporal association with production activity suggest that the earthquake was in fact induced. The timing of the 22 October earthquake, within about a year of initial development of the northwesternmost edge of the field, further suggests that in addition to production volume, the timing of the earthquake might have been controlled in part by drilling and production in

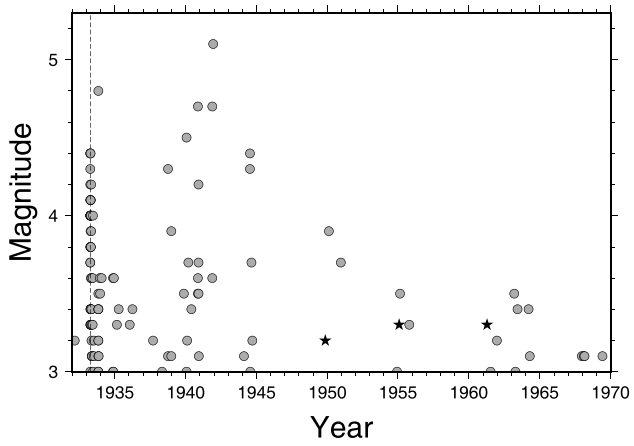

Figure 12. Timeline of $M_L \geq 3.0$ earthquakes (gray dots) in region shown in Figure 10. The shallow events analyzed by Kovach (1974) also shown (black stars). Dashed line indicates time of 1933 Long Beach earthquake.

proximity to the W-1 and W-2 fault strands, possibly including the drilling of a well that penetrated basement rock at a depth of 3.8 km. Although there was no production below depths of ≈2 km, it is possible that the well penetrated the fault directly. While drilling through faults is not uncommon and does not generally cause earthquakes, it can perturb locally the fluid and/or pressure balance within the fault zone.

The temporal and spatial proximity of the 22 October and 14 November earthquakes suggests strongly that the latter event was triggered by the former. Assuming a generic California aftershock model (e.g., Felzer et al., 2003), for example, there is a 3% chance that a *M*4.7 earthquake will be followed by a *M*5 or larger earthquake within the next 30 days. It is impossible to determine whether the spatial proximity of the 14 November earthquake to the Torrance field (Figure 4b) is coincidental or not. If, however, the earthquake was a natural triggered event, and one accepts the conclusion that the foreshock was induced, the occurrence of the 14 November earthquake demonstrates that induced earthquakes can potentially trigger larger tectonic mainshocks. Van der Elst et al. (2013) moreover conclude that regions with induced seismicity are more prone to triggered earthquakes. The 14 November 1941 earthquake could thus have been triggered by its foreshock yet still associated with oil production in the Torrance field.

4. Modeling

4.1. Development of the Wilmington and Adjacent Oil Fields

The inferred spatial and temporal association between the earthquakes analyzed in this study and active oil fields motivates us to use established modeling methods to further explore the hypothesis that the earthquakes might have been induced by oil production. We first review briefly the development of the Wilmington oil field as well as activities in neighboring fields during the 1930s–1940s.

The Wilmington oil field was discovered in 1932, although not developed until 1937 (Crown, 1941; Figure 13). As described by Crown (1941), the Wilmington field structure is classed as an anticlinal fold with a main axis trending NW-SE, cut by a series of transverse faults on which displacement ended before the end of the Pliocene period. The discovery well, Watson No. 2, was drilled in Section 29, Township 4S, Range 13W (33.7936°N, 118.2648°W, by Ranger Petroleum Corporation, in January, 1932; Figure 13). At the time, this well, which produced only a modest volume of oil, was considered to be within an extension of the Torrance field (Crown, 1941). Production within the Wilmington field effectively began with the completion of well No. Securities 1 in June 1936. The drilling boom was sparked by the completion of well Terminal No. 1 in December, 1936, which was drilled down to Franciscan Schist basement at 2.1 km (6787′) in Section 4, Township 4S, Range 13W (33.7673°N, 118.2410°W; Figure 13).

Production in the Wilmington field increased rapidly in 1937 and soon reached massive volumes (Figure 14). For example, through the first half of 1937 production in the field accounted for 7% of the 49 million barrels produced in all Los Angeles basin oil district; through the first half of 1938 production the field accounted for 33% of the 64 million barrels produced in the district. By the late 1940s, annual production within the Wilmington field alone rivaled the annual production in the entire district in the mid-1930s.

As documented in detail by Gilluly and Grant (1947), dramatic surface subsidence occurred within the Wilmington field during the 1940s as a consequence of production within the field. Kovach (1974) concluded that small, damaging earthquakes in 1947, 1949, 1951, 1954, 1955, and 1961 were associated with this subsidence (Figure 14b). Although Kovach (1974) does not provide precise epicenters, all estimated event locations are tightly clustered within the central subsidence bowl shown in Figure 13. Subsidence in the Wilmington area was increasingly well characterized through the 1940s (Gilluly & Grant, 1947), but Leypoldt and McHenry (1942) documents detectable subsidence of the Los Angeles inner harbor between 1936 and 1941 and concluded that subsidence likely extended about 5–6 km north from the coast. A tide gauge record from Long Beach Outer Harbor shows that subsidence began in 1937, reaching about 0.3 m by mid-1940 (Figure 13; Gilluly & Grant, 1947).

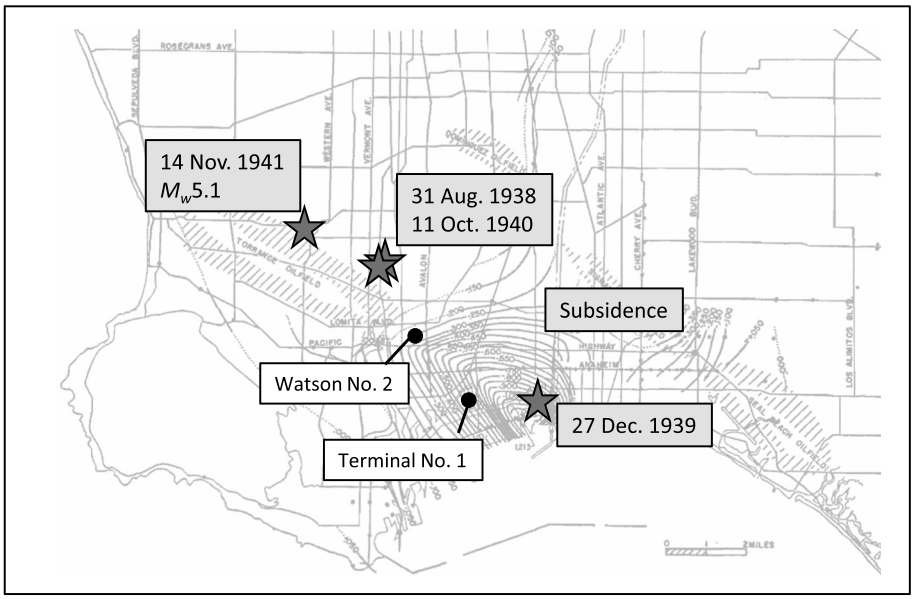

Figure 13. Contours indicate elevation changes in the Long Beach area between 1933 and 1934 and June-July 1941 determined by leveling (recrafted from Gilluly & Grant, 1947). The stars indicate preferred epicenter of earthquakes (dates labeled); the black dots indicate location of wells discussed in text.

Rapid development of the Wilmington oil field was spurred by demand for oil to support the war effort. In the words of Musser (1942; page 53), "The present war, referred to by many authorities as an Oil War, makes [the Wilmington] field doubly important with its monthly production in excess of two and one-half million barrels." Production in many other Los Angeles fields also increased through the 1930s, first as the country emerged from the Great Depression, and then by the need for oil to support the war effort. In many cases, wells were deepened in fields where more shallow production horizons had become depleted (see Table 4). Three of the earthquakes analyzed in this study occurred in proximity to the Torrance/Wilmington fields, within a few months to a few years following a rapid increase in production in the field: 31 August 1938, 11 October 1940, and 14 November 1941 (Figure 14a). In the following section we consider the predicted stress and change changes associated production in oil fields in the southwest Los Angeles basin.

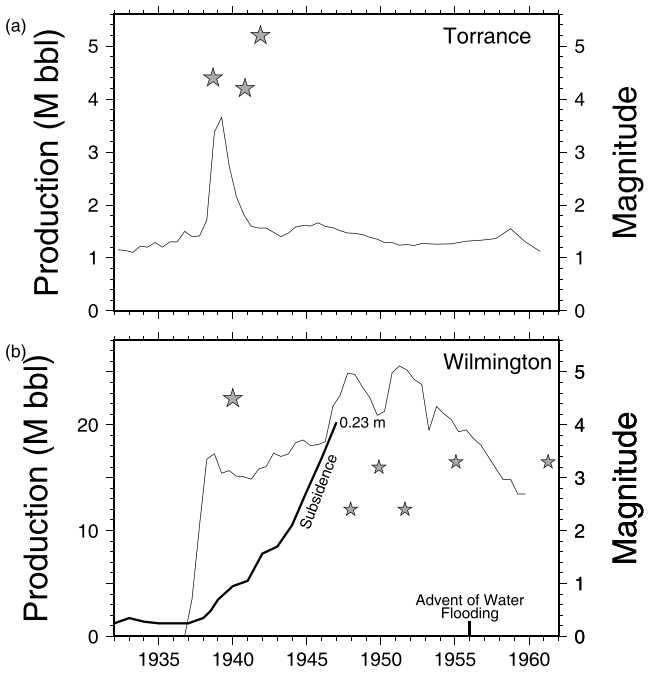

Figure 14. (a, top). Oil production within the Torrance oil field (millions of barrels; thin black line), reported biannually (see Data and Resources); the stars indicate times of earthquakes near the field (b, bottom) Oil production in the Wilmington field (thin black line) and differential subsidence of Long Beach Harbor (thick black line; data from Gilluly & Grant, 1947). The large star indicates 1939 earthquake; the small stars indicate shallow slump earthquakes analyzed by Kovach (1974).

4.2. Modeling Stress, Strain, and Displacement Associated With Oil Extraction

In this section we use available industry data (Table 5) quantify the geometry and amplitude of strain changes associated with oil production in the Wilmington and adjacent fields. To investigate deformation in the region of an oil field, we assume an elastic half-space with no layering. In comparisons between observed and synthetic surface deformation we impose subsurface displacements (convergence) at the depth of the oil horizons and compute surface displacements assuming uniform elastic conditions. In these circumstances the effects of weaker surface rheologies have relatively minor influence of modeled surface displacements. For a specified deflation at depth, depth-dependent elastic properties are very poorly constrained and will change the amplitude of predicted stresses but not the general features of their spatial distribution.

Table 4
Production Depths

Field	A (m)	B (m)	AB (m)	C (m)	D (m)	CD (m)	Z_B
Torrance	1,524	1,600	1,500	–	–	–	–
Rosecrans	2,300	2,350	2,300	2,500	2,600	2,550	–
Dominguez Hills	2,134	2,200	2,150	–	–	–	–
Long Beach	650	2,800	1,725	3,200	3,400	3,300	4,200
Seal Beach	800	1,300	1,050	1,500	2,700	2,100	4,200
Sunset Beach	2,200	2,600	2,400	2,700	3,200	2,950	4,500
Huntington Beach	400	1,400	900	1,600	2,000	1,800	3,100
El Segundo	–	–	–	2,100	2,300	2,200	
Newport	400	800	600	1,400	1,800	1,600	4,000
Wilmington	650	2,250	1,450	–	–	–	2,300

Note. Approximate field production depths (m) from Mayuga (1970) and Foster (1954). Columns A and B and C and D indicate the upper and lower bounds of early shallow, and later deeper production fields respectively. AB indicates mean of A and B depths; CD indicates mean of C and D. Z_B indicates depth to basement.

We apply a regional strain field to emulate the general stress conditions of the Los Angeles basin (e.g., Toda et al., 2005), and the stresses developed from subsurface fluid extraction are superimposed on the background state of stress. The models embed elastic dislocations, to the edges of which dislocation-normal displacements are imposed. A realistic convergence with displacements tapering to low values at the tips of each dislocation is implemented. We then calculate the geographic distribution of the resulting strain in the surrounding rocks, from which it is possible to determine shear and dilatational stress making simple assumptions for modulus and internal friction. We use the term *extensional dilatational strain* to refer to positive volume dilation; contractional dilatational strain refers to volume contraction. We used the elastic calculations of Okada (1987) as implemented in Coulomb 3.2 (Toda et al.) to compute stresses. In such models, a rectangular, approximately horizontal dislocation with finite length thus emulates an oil horizon collapsing as a result of oil extraction.

As a simplification, we model dislocations as rectangular deflating sources with width equivalent to the extraction-width of the oil horizon (3–6 km) and length determined by the length of the producing anticline. Since many hundreds of wells simultaneously pump numerous fault-confined reservoirs along each anticline with different rates of extraction, we make the further simplification that the rectangular region acts as an evenly depleted uniform source. Our resulting simplified geometries are rectangular in map view with aspect ratios of one to five. To avoid unrealistically large stresses near the edges of the depleting reservoirs, we maximize convergence near their center and taper the convergence to fractional values near the edges with an approximately elliptical spatial distribution.

Subsurface compaction results in subsidence of the surface above the oil field, and in the case of the Wilmington and Huntington Beach oil fields it is possible to approximately constrain the length and width of the depleted reservoir using the areas of surface subsidence mapped by leveling (Giluly & Grant, 1941; Castle & Buchanan-Banks, 1989). By 1939, 36 cm of surface subsidence had been observed in the Wilmington field, with a rate of subsidence increasing to 30 cm/year in 1946, peaking at a 71 cm/year in

Table 5
Field Areas and Production Volumes

Field	Area (km^2)	V_{1935} (km^3)	T_{1935} (m)	V_{1941} (km^3)	T_{1941} (m)	k	D_{1935} (m)	D_{1941} (m)
Torrance	26.56	0.012	0.46	0.02	0.71	0.15	0.069	0.106
Rosecrans	2.60	0.007	2.77	0.01	4.78	0.01	0.028	0.048
Dominguez Hills	4.64	0.012	2.59	0.03	5.71	0.01	0.026	0.057
Long Beach	5.94	0.102	17.16	0.17	29.10	0.01	0.172	0.291
Seal Beach	1.19	0.016	13.05	0.03	24.50	0.01	0.131	0.245
Huntington Beach	11.58	0.038	3.30	0.07	5.78	0.05	0.165	0.289
Wilmington	—	—	—	0.02	1.46	0.25	—	0.364

Note. Volume (km^3) in 1935 and 1941, V_{1935} and V_{1941}, converted to equivalent oil layer thickness, T_{1935} and T_{1941} (m), and adjusted layer deflation thickness, D_{1935} and D_{1941} (m), using empirical constants, k, as discussed in the text.

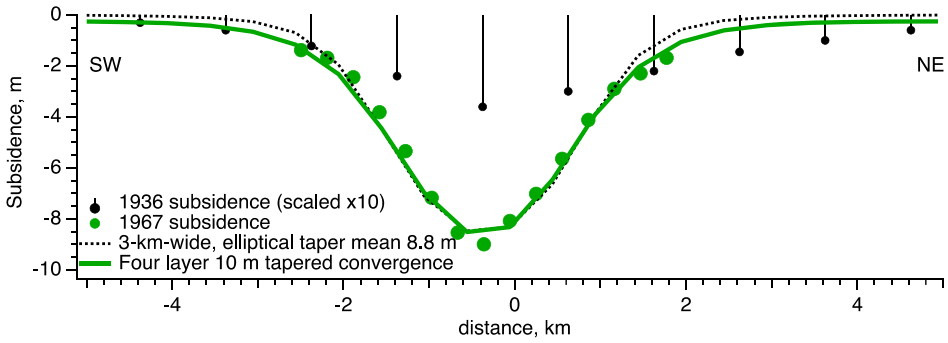

Figure 15. Subsidence observed in a NE profile across the Wilmington field 1934–1936 (black sticks with circles x10) and 1934–1967 (green circles) compared to synthetic subsidence from two deflating dislocation geometries. The best single-dislocation fit is 3-km-wide and 4-km-long at 910-m depth with mean 10-m deflation. An improved fit is obtained from four stacked dislocations between 760- and 1,010-m depth, widening downward from 3.0 to 5 km with mean total deflation of 10 m.

1951 (Giluly and Grant, 1941). The subsidence rate dropped aver 1951 due to a decrease in oil production (Mayuga, 1970), but net ground subsidence continued to increase. Simple models that approximately emulate the width and breadth of the surface subsidence and the maximum depression above the Wilmington field in 1936 and 1967 are illustrated in Figure 15. Between 1945 and 1949, compaction within the Wilmington field occurred primarily between 760- and 1,050-m depths, suggesting 25×10^{-3} vertical strain contraction within the oil producing horizon, with extension of $\approx 10^{-3}$ from 760 m to the surface (Mayuga, 1970). Models that emulate this 290-m-thick zone of compaction using a single deflating, horizontal, rectangular dislocation at 910-m depth fit the central region of subsidence well but underestimate subsidence beyond ±2 km from its center. A more complex four-layer model with mean, but tapered total inflation of 10 m, with downward increasing widths of 3.0, 3.6, 4.2, and 5 km, at depths of 766, 820, 915, and 1,010 m, approximates both the narrow central subsidence and subsidence beyond ±2 km. This subsurface geometry approximates the downward widening limbs of the anticline oil trap, although it is not a unique solution.

General modeling results are illustrated in Figure 16, including the strain and stress changes associated with production from a single horizon (Figures 16a and 16b) and the predicted stress change from stacked reservoirs at different depths (Figure 16c). Although the details of strain changes within 3 km of the edge of a producing oil field depend on its depth, the lateral reach of dilatational strain changes does not substantially increase when the deflation occurs at depth or whether it is evenly distributed over multiple stacked deflating horizons (Figure 16c).

We plot dilatational strain on the left hand panels of Figure 3 since this illustrates both the observed vertical strain fields (conventionally referred to as ε_{zz}) and the surface displacement fields used to constrain the models. We do not consider pore pressure changes at hypocentral depths, which in general are expected to be an order of magnitude greater than static stress changes if the causative faults are in direct hydrologic communication with the reservoir and enough time elapses for pore pressure effects to reach nearby faults (e.g., Roeloffs, 1996). Rather we treat the reservoir as a hydrologically isolated poroelastic medium to focus on modeling the expected reach of (instantaneous) static stress changes that could have perturbed faults before pore pressure diffusion effects became significant or were blocked by lower permeability underlying fault seals. A strain of 10^{-4} is chosen as a contour since strain-drops exceeding 10^{-4} correspond to the average ultimate strain at failure released by earthquakes worldwide (e.g., Bilham et al., 2017).

To model the overall effects of production in the southwest Los Angeles basin, we use available industry data for each field. The difference between the volume of fluid (oil plus water) removed and reservoir volume lost due to modeled subsurface reservoir deflation is caused by the resistance to contraction of the drained reservoir due to its dry bulk modulus and by the shear strength of the adjacent and overlying rocks; the details are expected to vary between different fields. For a specified reservoir depth and area, we calculate the decrease in reservoir thickness from the surface subsidence assuming elastic half-space conditions, and derive a ratio, *k*, for the inferred subsurface reservoir volume change relative to the volume of fluid removed. The

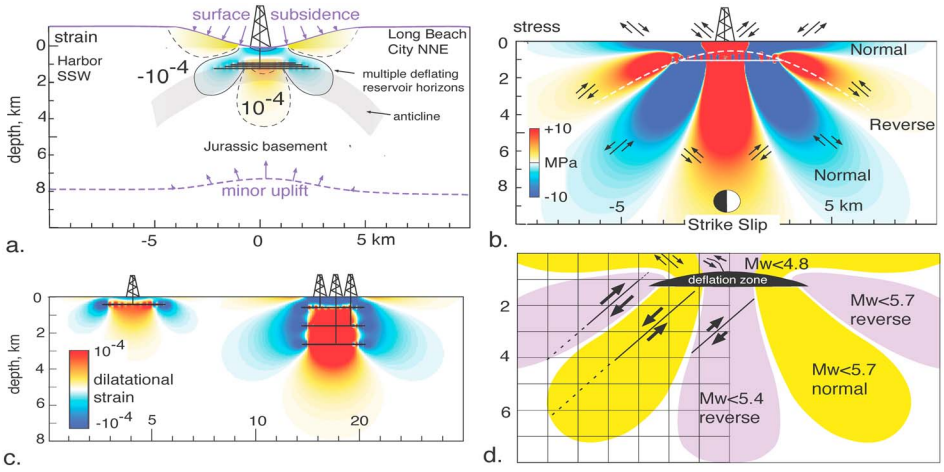

Figure 16. Sections across the Wilmington anticline showing (a and c) dilatational strain (negative indicates contraction) calculated from 8.8 m maximum subsidence tapering to zero at ±5 km from center of depression. Observed surface subsidence and calculated subsurface uplift are shown schematically in purple (<10-μm uplift at 8-km depth). (b and d) Regions of enhanced Coulomb failure for optimal faulting mechanisms as indicated (such that positive stress change favors reverse faulting and negative stress change favors normal faulting). By 1936 maximum Coulomb stress exceeded 1 MPa in the Jurassic basement 2.5 km directly below the field. Figure 3c illustrates the relatively minor increase in lateral reach of dilatational strain associated with stacked reservoir depletion (right portion of figure), and Figure 16d illustrates the approximate maximum magnitudes attainable with dip-slip ruptures if those ruptures are confined to the zones where their sense of faulting is favored in the stress field induced by reservoir depletion.

subsurface volume change required to emulate the 1967 maximum Wilmington subsidence of 8.8 m assuming a 4-km, along-strike extraction zone and the four-layer geometry described above is inferred to be 120×10^6 m^3, but after 1952 both oil production and subsidence rates had been decreasing, and by 1959 water injection volumes had exceeded oil extraction volumes (Mayuga, 1970). Hence, we use pre-1949 subsidence and fluid extraction data to estimate the constant, k. The 1941 extraction volume and subsurface reservoir area yield an equivalent thickness of fluid layer removed of 1.46 m. The maximum surface subsidence of 36 cm observed above the Wilmington oil field by 1939 (Gilluly & Grant, 1947) is approximately equal to one fourth the calculated subsurface layer thickness change; hence, we derive $k = 0.25$. For the Huntington Beach and Long Beach oil fields k can be approximated (≈0.05 and ≈0.01, respectively) from the 1926–1932 observed subsidence and fluid extraction volumes reported by Castle and Buchanan-Banks (1989). For fields where surface subsidence was not measured, with one exception, we use $k = 0.1$ to convert calculated fluid thickness changes to subsurface deflation (Table 2). The exception is the Torrance oil field, which might be expected to have the same k value as the adjacent Wilmington field. For this field, however, we assume $k = 0.15$, which is somewhat less than the Wilmington value, because grain size and layer thicknesses in the oil reservoirs between Wilmington and Torrance are reported to reduce northwestward (Elwany et al., 1988).

The Coulomb stress enhancement at 5-km depth from oil fields in the study area for the 1935 and 1941 epochs are shown in Figure 17. The predicted effects of the 1933 Long Beach earthquake are superimposed in the bottom panels. To calculate the Coulomb stress change associated with this earthquake, we assume mean slip of 0.8 m with a 10×17 km^2 rupture plane Hauksson and Gross (1991) with slip tapering to low values near the ends of the fault.

While the locations and mechanisms of the moderate earthquakes analyzed in this study are not constrained well enough to explore the detailed consistency of the stress change results with each earthquake, it is illuminating to consider the magnitude of predicted stress changes in the vicinity of each event. Notably, significant stress change extends to approximately twice the depth of the producing horizon, well into basement rock (e.g., Figure 16b). Our models confirm the general result of Soltanzadeh and Hawkes (2009) that dilatational strain changes decay quite rapidly to below 10^{-4} strain approximately 2 km from the nearest point of the extracting horizon. At distances of 5 km, maximum strain changes are less than 10^{-5}. Coulomb failure stress changes within 2 km of each active oil field exceed 1 MPa, decaying by an order of magnitude at

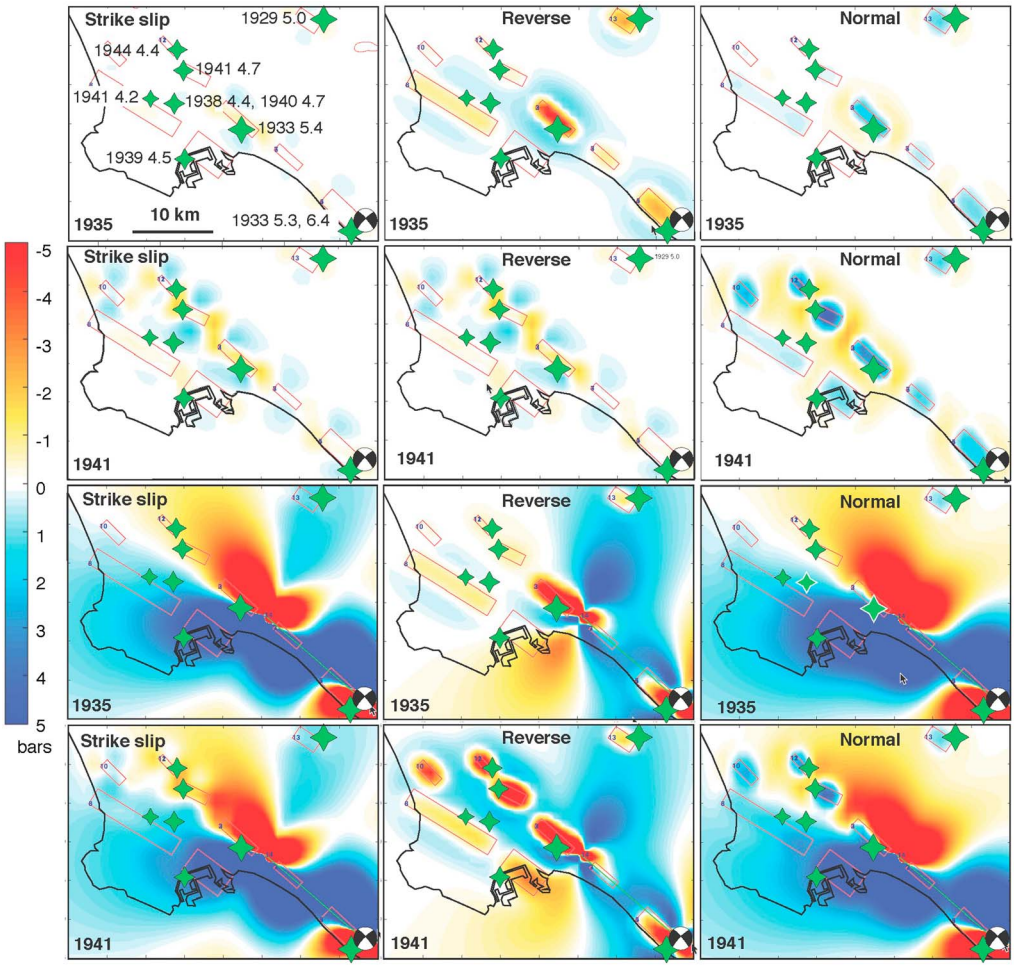

Figure 17. Coulomb strain changes at 5-km depth in (first row) 1935 and (second row) 1941 for optimum oriented (left column) strike-slip, (middle column) reverse, and (right column) normal faulting, respectively, using simplified production depths (Table 4) and reservoir geometries, and calculated subsurface deflation (Table 5). Preferred earthquake locations (green stars) all occur within 2–5 km of an oil field. The oil fields are modeled as rectangles as depicted. In the lower six panels, stress changes due to production (as described above) are added to estimated Coulomb stress changes at 5-km depth from the 1933 Long Beach earthquake.

distances exceeding 5 km. For contiguous parallel oil fields the shallow regions of tensile dilatation and the regions of subsurface contraction (blue) coalesce, but the geometry of the axial regions of enhanced strike-slip Coulomb failure directly below each field is unaffected.

While the results illustrated in Figure 17 depend on a number of assumptions, some first-order conclusions can be drawn. First, as noted, dilatational strain near oil fields are significant to distances of the order of 2–4 km from the edges of each field. By 1941, strike-slip and reverse faulting was encouraged directly beneath many fields, with stress changes upwards of 0.1 MPa; dip-slip faulting was encouraged around the peripheries of fields. Epicentral locations are uncertain to at best a few kilometers; however, the preferred locations for most of the earthquakes analyzed in this study are near the edges of an oil field within these zones. Investigations of triggered earthquakes associated with dynamic and static stress changes have concluded that triggered seismicity is typically associated with stress changes of 0.1 MPa or greater (e.g., Gombert et al., 2001; Toda et al., 1998); that is, stress changes of this magnitude have been shown to significantly promote, although not necessarily to always cause, frictional failure.

With the exception of the earthquakes that ruptured borehole casings in an (inferred) reverse faulting sense, the focal mechanisms of the moderate earthquakes analyzed in this study are unknown. There is, moreover,

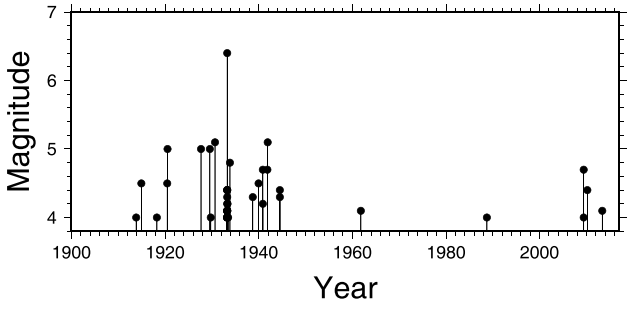

Figure 18. Timeline of magnitude 4 and larger earthquakes in the inset region in the southwestern Los Angeles basin (inset region in Figure 1).

little if any constraint on the hypocentral depths of most of the events. We therefore cannot consider in detail whether the actual mechanism of each moderate earthquake is consistent with the predicted style of faulting.

The spatial distribution of predicted stress change (e.g., Figure 16d) is also interesting to consider. Although large stresses are generated above, within, and adjacent to production zones, lobes of increased stress promoting a particular mechanism of rupture are limited in spatial extent and surrounded by regions where the same type of rupture is inhibited. Thus, if unstable rupture is induced by positive stress change, fault rupture lengths will tend to be limited to 2–5 km, corresponding roughly to M_w5.4–5.8 (e.g., Wells & Coppersmith, 1994). Ruptures would grow larger only if dynamic slip-weakening effects (e.g., Andrews, 1985) were sufficient for unstable rupture to propagate through these contiguous regions The shallow depths of induced earthquakes will further lessen the likelihood of an induced earthquake growing, since stress changes would be concentrated at depths characterized by velocity-strengthening rheologies (e.g., Marone & Scholz, 1988).

5. Discussion

We have shown that there is a spatial and temporal association between the earthquakes analyzed in this study and oil industry activities in the southwest Los Angeles basin during the late 1930s and early 1940s. The elevated rate of moderate (and small) earthquakes between 1938 and 1944 began following a notable boom in oil production. Modeling provides quantitative evidence that by the late 1930s, uncompensated production from the Wilmington and adjacent field did perturb subsurface stress and strain sufficiently to potentially induce earthquakes. The elevated rate of seismicity is particularly evident in the inset region in Figure 1, that is, southwestern Los Angeles basin (Figure 18).

While the low rate of moderate earthquakes after 1960 supports the conclusion that widespread water flooding was successful in balancing subsurface pressures and therefore mitigating earthquake risk, the period of elevated seismicity clearly ended about 15 years before widespread waterflooding began. This observation can be plausibly explained by the proposed triggering mechanism. The effect of static stress changes associated with oil extraction will be countered by pore pressure effects that serve, generally, to reduce effective stress on adjacent faults (e.g., Healy et al., 1968); however, whereas the static stress and strain changes modeled in our study will be essentially instantaneous, pore pressure changes in the surrounding medium will be moderated by flow and consequently delayed. If production increases sharply, as it did in the late 1930s and early 1940s (e.g., Figure 14), the effects of static stress change are more likely to dominate in the short term.

6. Conclusions

Revisiting available macroseismic and strong motion data for moderate earthquakes in the Los Angeles basin between 1938 and 1944, we conclude that early instrumental locations of even well-recorded events can be grossly inconsistent with detailed macroseismic data. We therefore conclude that available, spatially rich macroseismic data can provide better constraints on epicentral location and relocate epicenters accordingly. While Hauksson et al. (2015) concluded that there was no evidence for significant induced earthquakes in the Los Angeles basin in the twentieth century, their study relied on instrumental catalog locations, which we have shown to be unreliable even for the largest earthquakes during this time period. Their study did also find an increase in the rate of $M \geq 2.5$ earthquakes between 1935 and 1945, although they did not consider the increase significant. Our study presents a more detailed consideration of the largest earthquakes between the early instrumental era (1934–1952) in southern California as well as a more extensive consideration of relevant oil industry activities. We show that increased activity in the southwest Los Angeles Basin between 1935 and 1933 cannot be explained as aftershocks of the 1933 Long Beach earthquake. A reconsideration of available instrumental and macroseismic information, including detailed documentation of oil well damage caused by the 22 October 1941 M_w4.7 Dominguez Hills earthquake, suggests that this earthquake was likely induced by oil production in the Dominguez Hill oil field between 1923 and 1941. The 14 November 1941 M_w5.1 Torrance

earthquake was likely triggered by the 22 October foreshock; the proximity of the latter event to the Torrance field suggests a possible association between the occurrence of this earthquake and production in the field. Available strong motion data and macroseismic data, while limited, are consistent with a shallow depth.

For the pair of 1941 earthquakes as well as the other $M_w > 4$ events analyzed in this study, we have demonstrated a spatial and temporal association between the earthquakes and oil production in adjacent fields. To further explore a possible causal relationship, we have used available industry and subsidence data to model the predicted strain and Coulomb stress changes associated with oil production in the southwestern Los Angeles basin. We show that frictional failure would have been encouraged beneath and on the periphery of active oil fields, with stress changes upward of 0.1 MPa at 5-km depth. The spatially complex, small-scale nature of stress changes associated with individual oil fields might, we suggest, tend to limit the length of induced ruptures and therefore magnitudes.

The conclusion that much of the significant seismic activity in the Los Angeles basin during the first half of the twentieth century might have been induced (Hough & Page, 2016; this study) suggests that the rate of natural tectonic earthquakes within the Los Angeles basin might be lower than previously estimated.

Data and Resources

U.S. Geological Survey "Did You Feel It?" data are available at http://earthquake/usgs.gov/earthquakes/dyfi/ (last accessed January 2017). Oil production volumes for California oil fields, generally reported biannually, are available from ftp://ftp.consrv.ca.gov/pub/oil/Summary_of_Operations/ (last accessed January 2017). Well locations were specified in State reports by Section, Township, and Range, based on the Public Land Survey System. Detailed well information is also available from the DOGGR web site: https://secure.conservation.ca.gov/WellSearch/, last accessed January, 2017). Scanned copies of *United States Earthquakes* reports are available from: ftp://hazards.cr.usgs.gov/NEICPDE/olderPDEdata/scans/US_earthquakes/

Acknowledgments
We thank Misha Trifunac for providing the digitized recordings of the 14 November 1941 earthquake, Shemin Ge and Karl Mueller for helpful discussions during the elastic modeling, and thank James Dewey, Andrew Barbour, Cliff Frohlich, David Simpson, Martha Savage, Stephen Hickman, Katherine Kendrick, Michael Diggles, and an anonymous reviewer for constructive review comments. Summaries of felt reports from published sources are provided in the supporting information; industry data gleaned from cited sources are summarized in Table 4.

References

Andrews, D. J. (1985). Dynamic plane-strain shear rupture with a slip-weakening friction law calculated by a boundary integral method. *Bulletin of the Seismological Society of America*, *75*(1), 1–21.

Bakun, W. H. (2006). Estimating locations and magnitudes of earthquakes in southern California from modified Mercalli intensities. *Bulletin of the Seismological Society of America*, *96*, 1278–1295.

Bakun, W. H., & Wentworth, C. M. (1997). Estimating earthquake location and magnitude from seismic intensity data. *Bulletin of the Seismological Society of America*, *87*, 1502–1521.

Barnds, R. M. (1964). Seventeen years of successful Pliocene water flooding, Dominguez Hills oil field, Los Angeles County, California, Soc. Petroleum Eng. of AIME California Regional Meeting, Paper number 1023, Los Angeles.

Barnes, R. M., & Bowes, G. H. (1931). Seal Beach Oil Field, in summary of operations, California Oil Fields, Oct.–Dec., 1930, 16:2, pp. 9-31, San Francisco.

Bilham, R., Mencin, D., Bendick, R., & Burgmann, R. (2017). Implications for elastic energy storage in the Himalaya from the Gorkha 2015 earthquake and other incomplete ruptures of the Main Himalayan thrust. *Quaternary International*, *461*, 3–21.

Bodle, R. R. (1946). United States earthquakes, 1944, Coast and Geodetic Survey Serial No. 682, U.S. Department of Commerce, 50 pp, Washington DC.

Bravinder, K. M. (1947). Los Angeles basin earthquake of October 21, 1941, and its effect on certain producing wells in Dominguez field, Los Angeles County, California. *Bulletin of the American Association of Petroleum Geologists*, *26*, 338–399.

Castle, R. O., & Buchanan-Banks, J. M. (1989). Vertical surface displacements along a part of the Newport-Inglewood zone of folds and faults, Los Angeles and Orange counties, California, Miscellaneous Field Studies Map *2088*; https://pubs.er.usgs.gov/publication/mf2088

Coast and Geodetic Survey (CGS) (1937). Abstracts of earthquake reports for the Pacific Coast and the Western Mountain Region, Department of Commerce, U.S. Coast and Geodetic Survey, San Francisco, CA (https://babel.hathitrust.org/cgi/pt?id=uc1.31210003187018; last accessed 4 May 2017)

Coast and Geodetic Survey (CGS) (1940). Abstracts of earthquake reports for the Pacific Coast and the Western Mountain Region, MSA-24 October 1 1939 to December 31, 1939, Department of Commerce, U.S. Coast and Geodetic Survey, San Francisco, CA (https://babel.hathitrust.org/cgi/pt?id=uc1.31210003187026;view=1up;seq=239, last accessed 15 May 2017).

Coast and Geodetic Survey (CGS) (1941). Abstracts of earthquake reports from the Pacific Coast and the Western Mountain Region, Department of Commerce U.S. Coast and Geodetic Survey, San Francisco, CA.

Coast and Geodetic Survey (CGS) (1942). Abstracts of earthquake reports from the Pacific Coast and the Western Mountain Region, Department of Commerce U.S. Coast and Geodetic Survey, San Francisco, CA.

Coast and Geodetic Survey (CGS) (1944). Abstracts of earthquake reports from the Pacific Coast and the Western Mountain Region, Department of Commerce U.S. Coast and Geodetic Survey, San Francisco, CA.

Crown, W. J. (1941). Wilmington Oil Field, in Summary of Operations, California Oil Fields, Annual Report of the State Oil and Gas Supervisor, July, 1940-June,1941, 26, 5–11, San Francisco.

Elwany, H., Johnson, J., Dill, R., & Flick, R. E. (1988). Offshore subsidence monitoring program and possible mitigation measures, report prepared for Macpherson Oil Co. (http://www.hermosabch.org/modules/showdocument.aspx?documentid=4334, last accessed 25 May 2017).
Felzer, K. R., Abercrombie, R., & Ekstrom, G. (2003). Secondary aftershocks and their importance for aftershock forecasting. *Bulletin of the Seismological Society of America*, *93*(4), 1433–1448. https://doi.org/10.1785/0120020229
Foster, J. F. (1954). Rosecrans and South Rosecrans oil field: California Div. Oil and Gas. *California Oil Fields — Summ. Operations*, *40*(2), 5–15.
Frame, R. G. (1952). Earthquake damage, its cause and prevention in the Wilmington Oil field, in Summary of Operations, California Oil Fields, January–June, 1952, v38:1, 5–16.
Frankel, A., Hough, S., Friberg, P., & Busby, R. (1991). Observations of Loma Prieta aftershocks from a dense array in Sunnyvale, California. *Bulletin of the Seismological Society of America*, *81*(5), 1900–1922.
Frohlich, C., & Davis, S. D. (2002). *Texas earthquakes* (p. 221). Austin: University of Texas Press.
Gilluly, J., & Grant, U. S. (1947). Subsidence in the Long Beach Harbor Area, California. *Geological Society of America Bulletin*, *60*(3), 461–530. https://doi.org/10.1130/0016-7606(1949)60(461:SITLBH]2.0.CO;2
Gombert, J. S., Reasenberg, P. A., Bodin, P. l., & Harris, R. A. (2001). Earthquake triggering by seismic waves following the Landers and Hector Mine earthquakes. *Nature*, *411*(6836), 462.
Graves, R. W., Pitarka, A., & Somerville, P. G. (1998). Ground-motion amplification in the Santa Monica area: Effects of shallow basin-edge structure. *Bulletin of the Seismological Society of America*, *88*(5), 1224–1242.
Gutenberg, B. (1943). Earthquakes and structure in southern California. *Geological Society of America Bulletin*, *54*(4), 499–526. https://doi.org/10.1130/GSAB-54-499
Hamilton, R. M., Yerkes, R. F., Brown Jr., R. D., Burford, R. O, & DeNoyer, J. M. (1969). Seismicity and associated effects, Santa Barbara region, in Geology, Petroleum Development, and Seismicity of the Santa Barbara Channel Region, California, U.S. Geol. Surv. Prof. Pap. 67, 47–68.
Hauksson, E., Gobel, T., Ampuero, J.-P., & Cochran, E. (2015). A century of oil-field operations and earthquakes. *The Leading Edge*, *34*(6), 650–656. https://doi.org/10.1190/tle34060650.1
Hauksson, E., & Gross, S. (1991). Source parameters of the 1933 Long Beach earthquake. *Bulletin of the Seismological Society of America*, *81*(1), 81–98.
Healy, J. H., Rubey, W. W., Griggs, D. T., & Raleigh, C. B. (1968). The Denver earthquakes. *Science*, *161*(3848), 1301–1310. https://doi.org/10.1126/science.161.3848.1301
Hough, S. E. (2014). Shaking from injection-induced earthquakes in the central and eastern United States. *Bulletin of the Seismological Society of America*, *104*(5), 2619–2626. https://doi.org/10.1785/0120140099
Hough, S. E., & Page, M. (2016). Potentially induced earthquakes during the early 20th century in the Los Angeles basin. *Bulletin of the Seismological Society of America*, *106*(6), 2419–2435. https://doi.org/10.1785/0120160157
Hudson, D. E., Brady, A. G., & Trifunac, M. D. (1975). Analysis of strong motion earthquake accelerograms, volume 4—Fourier amplitude spectra, report no. Earthquake Engineering Research Laboratory 75–101, California Institute of Technology, Pasadena, 277 pp.
Huguenin, E. (1939). Operations in district no. 1, 1941, in Summary of Operations, California Oil Fields, Annual Report of the State Oil and Gas Supervisor, July, 1939 – June, 1940, v 27, 42–49.
Hutton, K., Woessner, J., & Hauksson, E. (2010). Earthquake monitoring in Southern California for seventy-seven years (1932-2008). *Bulletin of the Seismological Society of America*, *100*(2), 423–446. https://doi.org/10.1785/0120090130
Jennings, C.W. (1994). Fault activity map of California and adjacent areas, with locations and ages of recent volcanic eruptions, California Department of Conservation, Division of Mines and Geology, Geologic Data Map 6, 1:750,000.
King, G. C. P., Stein, R. S., & Lin, J. (1994). Stress changes and the triggering of earthquakes. *Bulletin of the Seismological Society of America*, *84*, 935–953.
Klein, F. (2002). User's guide to HYPOINVERSE-2000, a Fortran program to solve for earthquake locations and magnitudes (no. 2002–171). US Geological Survey.
Kovach, R. L. (1974). Source mechanisms for Wilmington Oil Field, California, subsidence earthquakes. *Bulletin of the Seismological Society of America*, *64*(3), 699–711.
Leypoldt, H., & McHenry, J. R. (1942). Block pattern of crustal movements in Long Beach. *Bulletin of the Seismological Society of America*, *32*(4), 269–276.
Los Angeles Times (1935). Mild tremor felt, 26 December 1935, page A3.
Los Angeles Times (1939). Mild tremor felt here, 28 December 1939, page A1.
Los Angeles Times (1941a). Loss in earthquake set at $350,000, 15 Nov. 1941, page A1.
Los Angeles Times (1941b). Quake repair work pushed, 16 Nov. 1941, page A2.
Los Angeles Times (1948). Terminal Island 'sinking' research gets underway, 15 May 1948, pg A1.
Los Angeles Times (1949). Navy's program to check sinking of shipyard balked, 23 December 1949, pg A1.
Los Angeles Times (1950). Sinkage of harbor causes no alarm, 15 May 1950, pg A2.
Los Angeles Times (1955). Long Beach seeks help to halt sinking of land, 29 September 1955, pg A1.
Los Angeles Times (1957). Repressurization plan hit by oil companies, 11 December 1957, pg B6.
Los Angeles Times (1958). Pact reached on Wilmington sinkage curb, 6 June 1958, pg A5.
Marone, C., & Scholz, C. H. (1988). The depth of seismic faulting and the upper transition from stable to unstable slip regimes. *Geophysical Research Letters*, *15*(6), 621–624. https://doi.org/10.1029/GL015i006p00621
Martner, S. T. (1948). The Dominguez Hills, California, earthquakes of June 18, 1944. *Bulletin of the Seismological Society of America*, *38*(2), 105–119.
Mayuga, M. N. (1970). Geology and development of California's giant—Wilmington Oil field, Amer. Ass. *Petroleum Geologists Special*, *A009*, 158–184.
McDonald, H. L., & Nessler, C. W. H. (1941). U.S. Geological Survey Topographic map, Torrance, Calif., Edition of 1934, reprinted 1941 with corrections, 1:24,000, N3348-W11818/6X8.
Musser, E. H. (1942). Operations in district no. 1., in Summary of Operations, California Oil Fields, Annual report of the State Oil and Gas Supervisor, July-Dec 1942, 28:2, 50–54, San Francisco.
Neumann, F. (1940). United States earthquakes 1938, Coast and Geodetic Survey, Serial No. 629, 58pp, Washington D.C.
Neumann, F. (1942). United States earthquakes 1940, Coast and Geodetic Survey, Serial No. 647, 75pp, Washington D.C.
Neumann, F. (1946). United States earthquakes 1941-1945, Coast and Geodetic Survey, Serial No. 655, 269 pp, Washington DC.
Okada, Y. (1987). Internal deformation due to shear and tensile faults in a half-space. *Bulletin of the Seismological Society of America*, *82*, 1018–1040.

Omori, F. (1894). *On the after-shocks of earthquakes* (Vol. 7). Tokyo: Tokyo University.
Richter, C. F. (1958). *Elementary seismology*. San Francisco, CA: W.H. Freeman.
Roeloffs, E. (1996). Poroelastic techniques in the study of earthquake-related hydrologic phenomena. *Advances in Geophysics*, *37*, 135–195.
Segall, P. (1989). Earthquakes triggered by fluid extraction. *Geology*, *17*(10), 942–946. https://doi.org/10.1130/0091-7613(1989)017<0942:ETBFE>2.3.CO;2
Segall, P. (1992). Induced stresses due to fluid extraction from axisymmetric reservors. *Pure and Applied Geophysics*, *139*(3-4), 535–560. https://doi.org/10.1007/BF00879950
Simpson, D. W., & Leith, W. (1985). The 1976 and 1984 Gazli, USSR, earthquakes—Were they induced? *Bulletin of the Seismological Society of America*, *75*(5), 1465–1468.
Soltanzadeh, H., & Hawkes, C. D. (2009). Assessing fault reactivation tendency within and surrounding porous reservoirs during fluid production or injection. *International Journal of Rock Mechanics and Mining Sciences*, *46*(1), 1–7.
Stover, C. W., & Coffman, J. L. (1993). Seismicity of the United States, 1568-1989 (revised), U.S. Geol. Surv. Prof. Paper 1527, 418 pp.
Suckale, J. (2010). Moderate-to-large seismicity induced by hydrocarbon production. *The Leading Edge*, *29*(3), 310–319. https://doi.org/10.1190/1.3353728
Toda, S., Stein, R. S., Reasenberg, P. A., Dieterich, J. H., & Yoshida, A. (1998). Stress transferred by the 1995 M_w = 6.9 Kobe, Japan, shock: Effect on aftershocks and future earthquake probabilities. *Journal of Geophysical Research*, *103*(B10), 24,543–24,565. https://doi.org/10.1029/98JB00765
Toda, S., Stein, R. S., Richards-Dinger, K., & Bozkurt, S. B. (2005). Forecasting the evolution of seismicity in southern California: Animations built on earthquake stress transfer. *Journal of Geophysical Research*, *110*(B5). https://doi.org/10.1029/2004JB003415
Ulrich, F. P. (1935). The California strong-motion program of the United States Coast and Geodetic Survey. *Bulletin of the Seismological Society of America*, *25*(1), 81–95.
Ulrich, F. P. (1938). Progress report for 1937 of the Seismological Field Survey of the Coast and Geodetic Survey. *Bulletin of the Seismological Society of America*, *28*(3), 205–215.
Ulrich, F. P. (1942). A progress report of the California seismological program of the Coast and Geodetic Survey, in the western United States during 1941. *Bulletin of the Seismological Society of America*, *31*(2), 107–119.
Van der Elst, N. J., Savage, H. M., Keranen, K. M., & Abers, G. A. (2013). Enhanced remote triggering at fluid-injection sites in the Midwestern United States. *Science*, *341*(6142), 164–167. https://doi.org/10.1126/science.1238948
Wald, D. J., Quitoriano, V., Dengler, L., & Dewey, J. W. (1999). Utilization of the internet for rapid community intensity maps. *Seismological Research Letters*, *70*(6), 680–697. https://doi.org/10.1785/gssrl.70.6.680
Wells, D., & Coppersmith, K. J. (1994). New empirical relationships among magnitude, rupture length, rupture width, rupture area, and surface displacement. *Bulletin of the Seismological Society of America*, *84*, 974–1002.
Zoback, M. D., & Zinke, J. C. (2002). Production-induced normal faulting in the Valhall and Ekofisk oil fields. *Pure and Applied Geophysics*, *159*(1), 403–420. https://doi.org/10.1007/PL00001258